hydrology

MDPI

Article

Modeling Reliability Quantification of Water-Level Thresholds for Flood Early Warning

Shiang-Jen Wu [1,*], Hao-Wen Yang [2], Sheng-Hsueh Yang [3] and Keh-Chia Yeh [2]

[1] Department of Civil and Disaster Prevention Engineering, National United University, Miaoli 360302, Taiwan
[2] Department of Civil Engineering, National Yang-Ming Chiao Tung University, Hsinchu 300093, Taiwan
[3] Disaster Prevention & Water Environment Research Center, National Yang-Ming Chiao Chiao Tung University, Hsinchu 300093, Taiwan
* Correspondence: sjwu@nuu.edu.tw

Abstract

This study proposes a framework, the RA_WLTE_River model, for quantifying the reliability of flood-altering water-level thresholds, considering rainfall and runoff-related uncertainties. The Keelung River in northern Taiwan is selected as the study area, and associated hydrological data from 2008 to 2016 are applied in the development and application of the model. According to the results from the model development and demonstration, the average and maximum rainfall intensities, roughness coefficients, and maximum tide depths exhibit a significant contribution to the reliability quantification of the estimated water-level thresholds. In addition, empirically based water-level thresholds can achieve the goal of rainfall-induced flood early warning, with a high likelihood of nearly 0.95. Additionally, the probabilistically based water-level thresholds derived from the described reliability can efficiently ensure consistent flood early warning performance at all control points along the river.

Keywords: water-level threshold; rainfall-induced flood early warning; multivariate Monte Carlo simulation; reliability quantification

1. Introduction

In recent years, extreme rainfall events have frequently caused severe floods, significantly increasing the risk of damage to people's lives and property. Flood-controlled hydraulic structures, such as the embankment, pumping station, and reservoir, play an essential role in flood prevention and mitigation. However, due to climate change, uncertainties in these structures' hydrological, hydraulic, and topographical characteristics increase the risk of failure in flood-controlled performance (e.g., dike overtopping). Nevertheless, their flood-controlled performance can be boosted by rehabilitating the hydraulic structures; however, while this would incur a large cost, it would hardly achieve the goal of ultimately reducing the failure risk, as it would considerably increase the variation in the uncertainties mentioned above.

In general, flood early warning can be implemented using data-derived and model-created methods [1]. For example, in data-derived methods, floods can be alerted when real-time observations exceed a desired threshold [2–7]. However, hydraulic factors (e.g., river-channel roughness coefficient) and topographical features (e.g., riverbed elevation and cross-section) might significantly affect the estimation of rainfall-induced river runoff and water levels [4,8–10]. Namely, the reliability and accuracy of flood early warning might

Check for updates

Academic Editor: Fabio Castelli

Received: 25 October 2025
Revised: 14 December 2025
Accepted: 6 January 2026
Published: 14 January 2026

Copyright: © 2026 by the authors. Licensee MDPI, Basel, Switzerland. This article is an open access article distributed under the terms and conditions of the Creative Commons Attribution (CC BY) license.

be affected by various sources of uncertainty in the rainfall–runoff–river process [11–14]. Therefore, by comparing water-level thresholds with observed river stages, flood early warning can be efficiently achieved. In general, when river stages reach the water-level thresholds, they exceed the specific target levels after a known time stage (the warning time), which is commonly the maximum water level for the specified return period [13]. In addition to the above uncertainties, the early altering performance of the flood is more likely to be influenced by the spatial density of the measurement stations [14].

Concerning the model-created flood warning operation, flood simulation should be comprehensively accomplished via physically based numerical models, including rainfall–runoff analysis and river routing, alongside the observed and forecasted hydrological data (e.g., precipitation, tide depth, and boundary runoff); a flood can be altered based on the resulting water levels and inundation depths at the target locations [4,15–20]. The physically based numerical model can provide detailed information on the flood simulation, including runoff, induced water-level hydrographs, and the flooded area; thus, by comparing the resulting river-stage forecasts with dike heights or water-level thresholds, early flood warning can be conducted. However, to achieve flood early warning, a variety of hydrological, hydraulic, and topographical data are required to configure numerical models; when configured via a physically based numerical model, the resulting flood simulation should require substantial computational time, depending on its temporal and spatial resolutions [21–24]. In addition to physically based flood simulation models, which may be associated with parametric uncertainty and computational complexity, AI-created models are frequently applied in flood early warning [11,25–29]. Despite AI-created models being more efficient than physically based models in flood simulation, massive training datasets and powerful processing capabilities are required during training and validation, which leads to high computational costs [30–32].

Overall, a group of physically based numerical models has been widely used to forecast and mitigate flood-induced disasters; nevertheless, data-derived water-level thresholds are commonly adopted in flood early warning operations and applied immediately, in comparison to river-stage observations, without incurring expensive computation time or powerful computing capability. Additionally, by collaborating with AI-generated models that rapidly forecast river stages, water-level thresholds can enhance the efficiency and performance of flood early warning systems. Therefore, data-derived water-level thresholds play an essential role in flood early warning operations, effectively providing primary flood alerts at specific river locations. However, it is well known that climate change and induced extreme events can cause significant variations in hydrological and hydraulic data, leading to uncertainties in the calibrated parameters of physically based and AI-created models [33]; accordingly, these uncertainties may affect the early warning performance of river-based water-level thresholds. Therefore, this study aims to model a reliability analysis to quantify the effects of the above uncertainties on the estimated water-level thresholds at specific locations along the river (named the RA_WLTE_River model). It is anticipated that the proposed RA_WLTE_River model can not only assess the reliability of the introduced water-level thresholds but also provide water-level thresholds with an acceptable likelihood (probabilistic-based thresholds) at the locations concerned along the river.

2. Methodology

2.1. Model Concept

As mentioned above, the proposed RA_WLTE_River model mainly provides a probabilistically based water-level threshold by coupling a conventional hydraulic–dynamic numerical model with an uncertainty/reliability analysis, subject to uncertainties in hydrological and hydraulic factors. Also, in response to uncertainties in the hydrological

and hydraulic factors with a correlation in time and space, several uncertainty and risk analysis methods have been proposed [34–37], which can be grouped into two types: the analytical approach and approximation methods. The analytical approach (i.e., the derived distribution method and Laplace and exponential transform techniques) can provide overall stochastic information on uncertainties in hydrological variables; however, their corresponding probability functions must be known in advance, which might be challenging when there are insufficient observations. Also, the functional relationships between mode outputs and uncertainty factors are necessary. Moreover, the commonly used approximation methods are the mean- and advanced first-order and second-moment (MFOSM and AFOSM) methods, Latin Hypercube Sampling (LHS), and Monte Carlo simulation (MCS). Among the above approximation methods, the advanced first-order second-moment (AFOSM) method primarily focuses on uncertainty and risk assessment under failure conditions; therefore, it is more appropriate for the safety assessment of flood-proofing systems [34]. Thus, the proposed RA_WLTE_River model allows for configuring the AFOSM to quantify and evaluate the reliability of water-level thresholds. In addition, using the AFOSM method, a relationship must be established between the uncertainty factors and the resulting model outputs [34]. Therefore, this study employs the correlated multivariate Monte Carlo simulation (MMCS) method [35] to reproduce a considerable number of uncertainty factors. After that, a significant number of water-level thresholds at specific locations along the river can be emulated via the hydraulic–dynamic numerical model with the generated uncertainty factors. Eventually, the reliability of the resulting water-level thresholds can be quantified in terms of exceedance probabilities using the uncertainty/reliability approach, incorporating the statistical properties of the hydrological and hydraulic factors. To efficiently proceed with the above reliability quantification, the exceedance-probability calculation equations are derived from logistic regression analysis using the relevant water-level thresholds and known uncertainty factors. The detailed methods and concepts applied in the development of the proposed RA_WLTE_River model are introduced as follows:

2.2. Estimation of River-Based Water-Level Thresholds

In general, river stages exhibit a high correlation in both time and space; thus, the determination of the current river stage should be influenced by the water levels at previous time steps during a rainfall-induced flood. Therefore, the flood-related water-level thresholds can be estimated by subscribing a target level (H_T), equal to the water level of a desired return period, from the expected stage at the control section, equal to the typical rising rate of the river stage ($\frac{\Delta H}{\Delta t}$) multiplied by a particular warning time t_W via the following equation [36]:

$$H_W^{t_W} = H_T - \left(\frac{\Delta H}{\Delta t}\right)_T \times t_W \quad (1)$$

The corresponding maximum water level at the time step (called the time-to-peak, t_P) to the control point is commonly defined as the typical one (H_T); also, the resulting rising rate $\left(\frac{\Delta H}{\Delta t}\right)_T$ can be obtained from the difference between the maximum water level at the time-to-peak (t_P) and at the time step ($t_P - t_W$) divided by the warning time (t_W). The above-described process for estimating the water-level threshold for a warning using Equation (1) is illustrated in Figure 1.

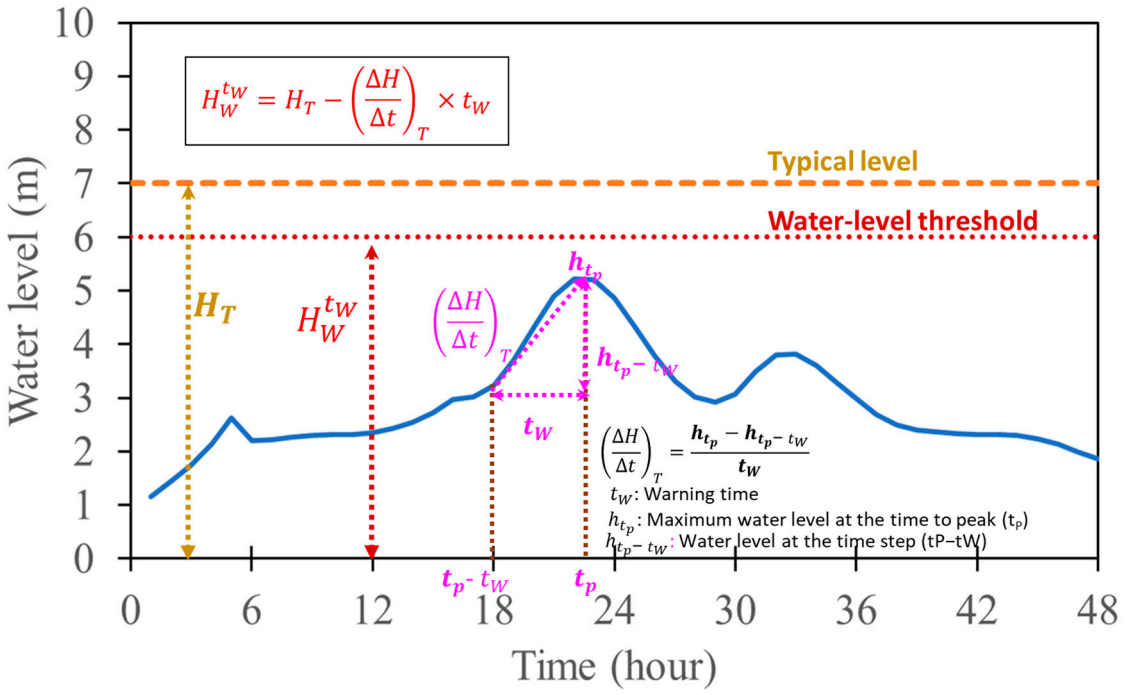


Figure 1. Schematic illustration of estimating the water-level threshold.

2.3. Simulation of Rainfall-Induced River Stages

In this study, to quantify the uncertainty of rainfall in time and space, a significant number of the rainstorms corresponding to sub-basins should be simulated. These sub-basin-based rainstorms can be achieved by combining the simulated rainfall characteristics at all grids in the study area via the stochastic model for generating the short-term rainfall (SM_GSTR) model [31]. Within the SM_GSTR mode, the sub-basin-based rainstorms should be characterized in advance into three rainfall characteristics: the rainfall duration, sub-basin rainfall depths (regarded as the spatial variates), and sub-basin storm patterns. The storm patterns comprise the dimensionless rainfalls at the various dimensionless times (treated as the spatio-temporal correlated variates). Using the SM_GSTR model, the sub-basin-based rainfall characteristics should be emulated via the Monte Carlo simulation with the correlated non-normal multivariate (MMCS) method [35], which is described in detail in Wu's study [31].

After generating the sub-basin-based rainstorms, the simulation of the river-based water-level thresholds can be implemented by coupling the river routing adapted in the hydraulic–dynamic numerical (SOBEK) model with the above-generated rainstorms. The SOBEK model is a sophisticated one-dimensional open-channel dynamic-flow and two-dimensional overland-flow modeling system (Sobek 1D-2D hydrodynamic model) [37]. Within the SOBEK model, the Sacramento Soil Moisture Accounting (SAC-SMA) model is used to estimate runoff based on boundary and lateral conditions. The SCA-SMA is a deterministic and semi-distributed hydrologic model with 18 hydrologic and soil-moisture-related parameters. Wu et al. [38] indicated that the SAC-SMA parameters, UZTWM, UZFWM, UZK, PCTIM, ADIMP, ZPERC, REXP, LZTWM, DF_L, and DF_P (see Table 1), which are calibrated via the modified genetic algorithm (called the GA-SA algorithm), contribute more sensitivity to the runoff estimation [38].

Table 1. Description of parameters of the *SAC-SMA* model [38].

Parameters	Description
UZTWM	Upper-zone tension water capacity (mm)
UZFWM	Upper-zone free water capacity (mm)
UZK	Upper-zone recession coefficient
PCTIM	Percent of impervious area
ADIMP	Percent of additional impervious area
ZPERC	Minimum percolation rate coefficient
REXP	Percolation equation exponent
LZTWM	Lower-zone tension water capacity (mm)
DF_L	Period of runoff distribution function
DF_P	Maximum ratio of the runoff distribution function

Overall, within the SOBEK model, the parameters used to estimate river runoff and stages should be reproduced by the MMCS method. Hence, using the generated rainstorms, a considerable number of the rainfall-induced river stages at concerned cross-sections can be obtained via the SOBEK model with the generated channel-based roughness coefficients at different cross-sections and inflow-based conditions, as well as the tide depths at the estuary. Eventually, a considerable number of simulated river-based water-level thresholds are attributed to the generated rainfall-related and runoff-related factors.

2.4. Identification of Uncertainty Factors Subject to River-Based Water-Level Thresholds

While conducting the reliability analysis, the uncertainty variables that may cause variations in the model outputs should be identified in advance [34,39]. In general, the runoff-induced water levels can be estimated using river routing and rainfall–runoff analysis, particularly during rainstorms. Consequently, the corresponding uncertainty factors for the water-level thresholds can be derived from these analyses. Therefore, in addition to the rainfall-related uncertainty factors, the parameters of the rainfall–runoff modeling (i.e., the SAC-SMA model) and the river-channel roughness coefficient are regarded as runoff-related factors. Moreover, the tide depth is commonly used as the downstream condition in river routing; therefore, it should be treated as an uncertainty factor. In summary, the relevant uncertainty factors for the estimated water-level thresholds are listed in Table 2.

Table 2. The uncertainty factors relying on the estimation of runoff and water level adopted in the proposed RA_WLTE_River model.

Hydrological Analysis Adopted	Uncertainty Factor	Definition
Rainfall–runoff and 1D river-stage routing	Rainfall-related factor	Rainfall duration Rainfall depth Storm pattern
	Runoff-related factor	Parameters of the rainfall–runoff (SAC-SAM) model Tide depth Riverbed roughness coefficient

2.5. Reliability Quantification of River-Based Water-Level Thresholds

Following the identification of uncertainty factors, reliability quantification should be achieved using the uncertainty–risk method, with a considerable number of estimated water-level thresholds for various warning times, considering the different combinations of the generated uncertainty factors [39]. Referring to Equation (1), the river-based water-level

thresholds are determined based on the dike height; an overestimated water-level threshold might cause the overtopping risk in terms of the exceedance probability as follows:

$$Exceedance\ probability = Pr\left(H_W^{t_W} > h_w\right) \tag{2}$$

where $H_W^{t_W}$ and h_w serve as the estimated water-level threshold and the potential threshold regarding a desired warning time t_W. Therefore, within the proposed RA_WLTE_River model, the reliability of the estimated water-level thresholds can be defined as

$$\text{Reliabilty} = Pr\left(H_W^{t_W} \le h_w\right) = 1 - Pr\left(H_W^{t_W} > h_w\right) \tag{3}$$

2.5.1. Advanced First-Order and Second-Moment AFOSM

To quantify the reliability of the above water-level threshold, the risk/uncertainty analysis (i.e., the advanced first-order and second-moment approach, AFOSM) is adopted. AFOSM is a well-known method used in hydrological and water resource reliability analysis [40–43]. Quantified via the AFOSM approach using the standard normal distribution with the first two statistical moments (mean and variance) of the desired uncertainty factors, the safety of structural components and systems can be evaluated from the resulting exceedance probability [44]. Hence, this study employs the AFOSM method to calculate the exceedance probabilities ($Pr\left(H_W^{t_W} > h_w\right)$) and to quantify the reliabilities of the river-based water-level thresholds of the warning time ($H_W^{t_W}$) (see Equation (5)) via the following equation:

$$\text{Reliability} = 1 - Pr\left(H_W^{t_W} > h_w\right) = 1 - Pr[Z_H > 0] = 1 - \Phi(-\beta)$$

$$Z_H = H_W^{t_W} - h_w,\ \beta = \frac{E(Z_H)}{s_{Z_H}} \tag{4}$$

where Z_H stands for the standardized variable of the water-level threshold, with mean $E(Z_H)$ and standard deviation s_{Z_H}; and $\Phi(\cdot)$ and β serve as the standard normal distribution and the reliability index, respectively. Using the AFSOM method, $E(Z_H)$ and s_{Z_H} can be calculated through the following equations:

$$E(Z_H) = H_{W,\theta^*} + \sum_{i=1}^{m} \left| \frac{\partial H_W^{t_W}}{\partial \theta_i} \right|_{\theta^*} \left(\mu_{\theta_i} - \theta_i^*\right) - H_W^{t_W}$$

$$s_{Z_H} = \sqrt{\sum_{i=1}^{m} \left(\frac{\partial H_W^{t_W}}{\partial \theta_i} \right)^2 \sigma_{\theta_i^*}^2} \tag{5}$$

where θ^* stands for the failure points of the ith uncertainty factor if the standardized variate $Z_H = 0$; μ_{θ_i} and $\sigma_{\theta_i^*}$ are the mean and standard deviation of the ith uncertainty factor, respectively; H_{W,θ^*} accounts for the water-level threshold estimated with the uncertainty factors' failure points; and H_W is the sensitivity coefficient of the ith uncertainty factor.

To proceed with risk quantification via the AFOSM method, a functional relationship between the model outputs and inputs is required in advance [34,43]. Thus, in this study, a functional relationship of the estimated water-level threshold of the warning time with the corresponding rainfall-related and runoff-related uncertainty factors can be defined as follows:

$$H_W^{t_W} = f\left(\theta_{Rain}, \theta_{Runoff}\right) \tag{6}$$

where $H_W^{t_W}$ denotes the water-level thresholds of the warning time (t_W), and θ_{Rain} and θ_{Runoff} serve as the rainfall-related and runoff-related factors, respectively. To calibrate the coefficients of the uncertainty factors in Equation (6), multivariate regression analysis is employed using a large number of corresponding estimated water-level thresholds for the generated uncertainty factors.

2.5.2. Logistic Regression Equation

In this study, by combining the AFOSM method with the above Multivariate Monte Carlo Simulation (MMCS) method, the reliability of the estimated water-level thresholds can be quantified using a large number of rainfall- and runoff-related factors; however, this approach would require substantial computational time. Therefore, to effectively quantify the reliability of water-level thresholds of the warning time (t_W), a logistic regression equation is configured within the proposed RA_WLTE_River model for calculating the exceedance probability ($Pr\left[H_W^{t_W} > h_w\right]$). The logistic regression analysis is widely used in hydrological and water resources analysis to derive a functional relationship between the occurrence probability of a dependent variable and a set of independent variables [44,45]. Accordingly, Equation (7) is derived from the logistic regression analysis under the specified magnitudes of the rainfall- and runoff-related uncertainty factors.

$$ln\left(\frac{Pr\left[H_W^{t_W} > h_w\right]}{1 - Pr\left[H_W^{t_W} > h_w\right]}\right) = \alpha_0 + \alpha_{H_W^{t_W}} H_W^{t_W} + \alpha_{\theta_{Rain}}\theta_{Rain} + \beta_{\theta_{Runoff}}\theta_{Runoff} \quad (7)$$

where θ_{Rain} and θ_{Runoff} denote the rainfall- and runoff-related factors with the corresponding regression coefficients, $\alpha_{\theta_{Rain}}$ and $\beta_{\theta_{Runoff}}$, respectively, and $\alpha_{H_W^{t_W}}$ stands for the regression coefficient of the water-level thresholds of the warning time t_W. Also, the exceedance-probability calculation equation can be utilized to estimate the probabilistically based water-level thresholds by rewriting Equation (7) as

$$H_W^{t_W} = \frac{1}{\alpha_{H_W^{t_W}}}\left[ln\left(\frac{Pr\left[H_W^{t_W} > h_w\right]}{1 - Pr\left[H_W^{t_W} > h_w\right]}\right) - \left(\alpha_0 + \alpha_{\theta_{Rain}}\theta_{Rain} + \beta_{\theta_{Runoff}}\theta_{Runoff}\right)\right] \quad (8)$$

2.6. Model Framework

In total, the proposed risk analysis for the river-based water-level thresholds (named RA_WLTE_River) is developed by coupling the uncertainty/reliability method (AFOSM) and a logistic regression equation with the hydraulic–dynamic model (SOBEK), using a set of generated rainfall- and runoff-related factors to account for their uncertainties. The detailed frameworks of the model development and application, referred to in Figure 1, are expressed below.

2.6.1. Model Development

Step (1): Collect the historical hydrological data (rainfall, runoff, and tide depth), topographical features (roughness coefficient and cross-section), and information on the hydraulic structures in the study area.

Step (2): Create the hydraulic–dynamic numerical (SOBEK) model based on the hydrological and topographical data, as well as the hydraulic structures, in which the parameters of the rainfall–runoff (SAC-SMA) model can be calibrated with the historical rainfall-induced runoff.

Step (3): Extract the observations of the rainfall- and runoff-related factors to calculate their statistical properties.

Step (4): Simulate a considerable number of rainfall- and runoff-related factors based on their statistical properties.

Step (5): Using the SOBEK model and the generated uncertainty factors in Step (4), achieve a significant number of river-stage hydrographs at various locations in the study area.

Step (6): Estimate the water-level thresholds of various warning times using Equation (1) with a noticeable number of river-stage hydrographs at multiple locations in the study area.

Step (7): Perform an uncertainty/reliability analysis to quantify the exceedance probability of the estimated water-level threshold using the AFOSM methods, considering a range of simulated water-level thresholds and their corresponding uncertainty factors.

Step (8): Derive the exceedance-probability calculation equations for quantifying the reliability of the estimated water-level thresholds via the logistic regression analysis.

2.6.2. Model Application

Within the proposed RA_WLTE_River model, the corresponding reliability to the specified water-level threshold can be quantified and evaluated using the exceedance-probability calculation equation, Equation (7), under the various combinations of the uncertainty factors concerned. In addition, the probabilistically based water-level thresholds can be determined using Equation (8) to achieve the desired reliability. The above application framework of the proposed RA_WLTE_River model is expressed below:

Step (1): Determine the uncertainty factors related to rainfall and runoff characteristics, considering the water-level thresholds for the desired warning times.

Step (2): Calculate the exceedance probabilities of the specific water-level thresholds at the different cross-sections subject to conditions of the sensitive rainfall- and runoff-related factors given using Equation (8).

Step (3): Evaluate the impact of the variation in the sensitive rainfall- and runoff-related factors on the estimated water-level thresholds based on the resulting exceedance probabilities from the change in the sensitive uncertainty factors.

Step (4): Estimate the probabilistically based water-level thresholds at various locations using Equation (8) with a given reliability. The frameworks of the above model development and application are shown in Figure 2.

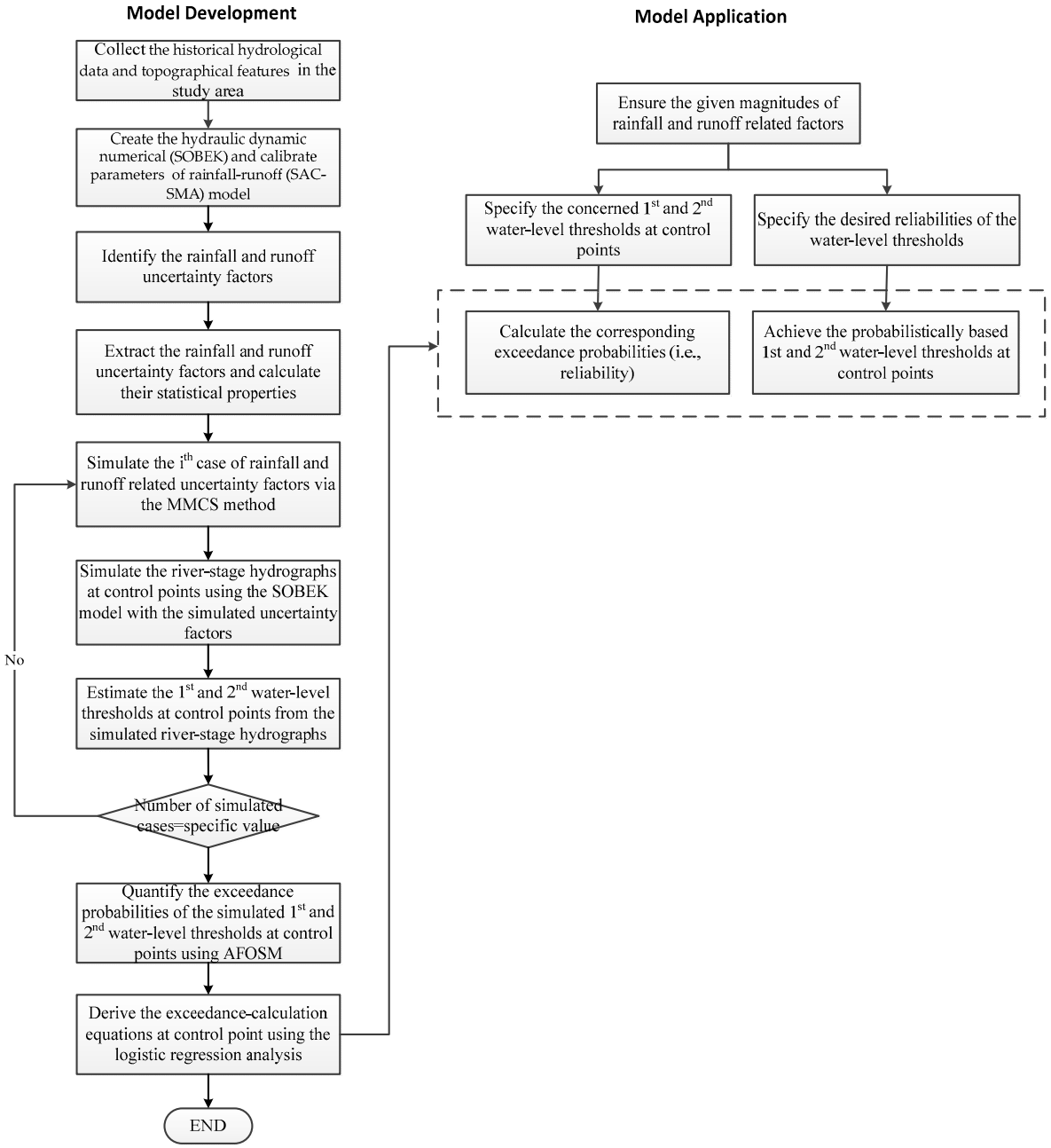


Figure 2. Development and application framework of the proposed RA_WLTE_River model.

3. Materials

3.1. Study Area

To introduce the development and demonstration of the proposed RA_WLTE_River model, the Keeling River watershed in north Taiwan, a branch of the Danshuei River that is associated with a variety of flood-controlled hydraulic structures and hydrological measurement gauges (12 water-level stations and 5 automatic rain gauges), was selected as the study area, as shown in Figure 3. The Keelung River starts in Jingtong Mountain and diverts the Danshuei River in the Kwantu area across the Ping-Shi township and Taipei County; the corresponding river length—and consequently the size of the study area—is around 86.4 km and 491 km^2, respectively. The flood-controlled hydraulic structures, including the Yuanshanzi flood diversion; the construction of dikes, water gates, and pumping stations; and the reconstruction of bank protection bridges, were designed and built in response to flood induced by a 200-year rainstorm. In addition, to estimate the

runoff hydrograph in the Keelung River, elevations at 128 cross-sections were surveyed, and 12 water-level gauge cross-sections were selected as control points. Their empirically based water-level thresholds were determined from the elevations of the left and proper levees for flood prevention and protection relative to historical flood-induced river stages, as shown in Figure 4.

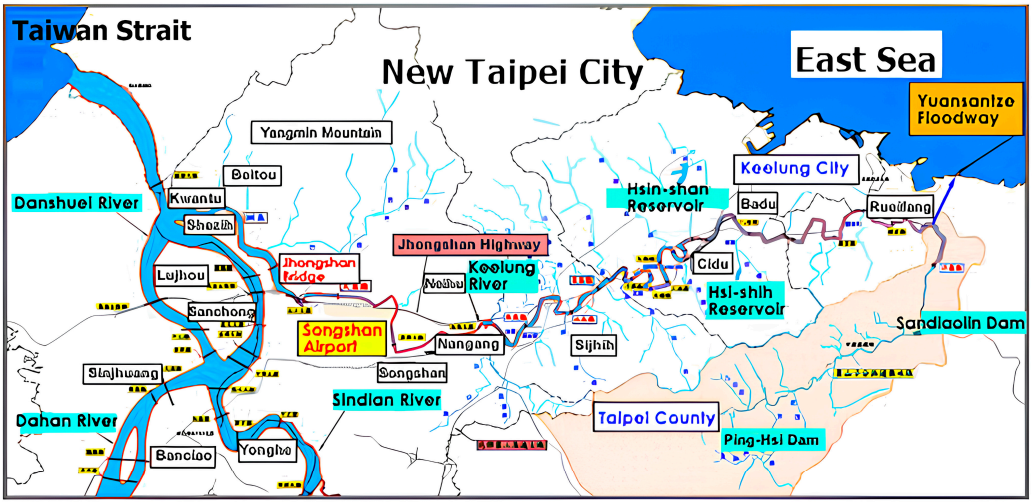
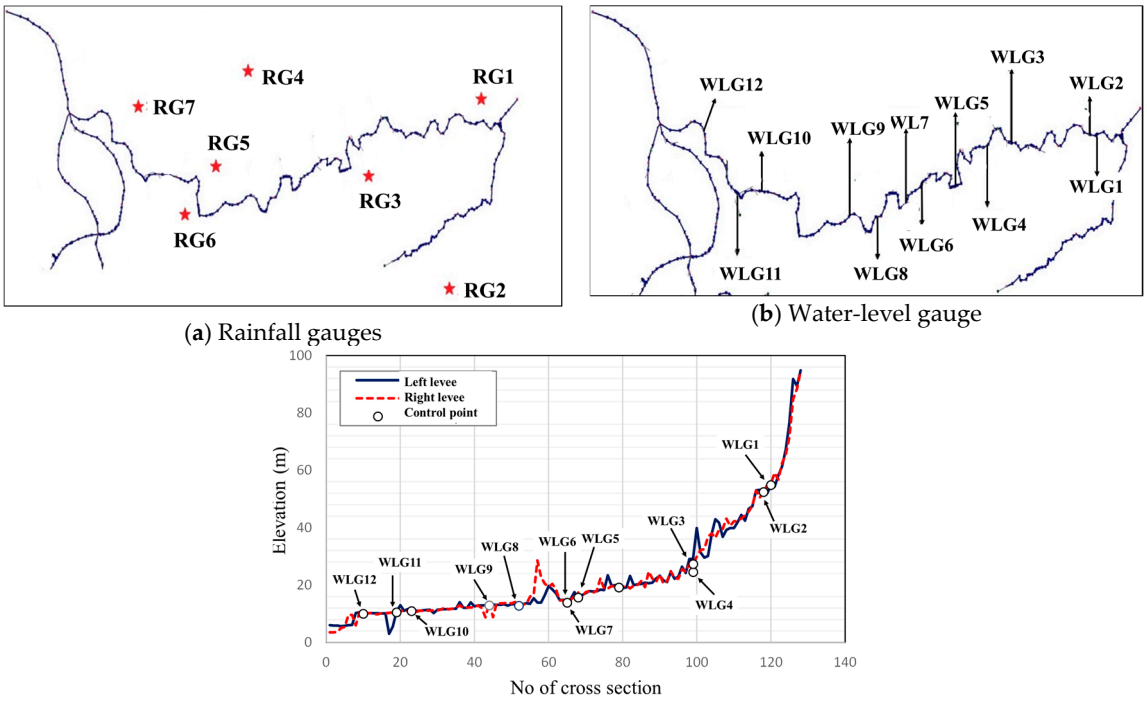


Figure 3. Keelung River watershed and neighboring basins [34].



(**a**) Rainfall gauges

(**b**) Water-level gauge

(**c**) Riverbed elevations at control points

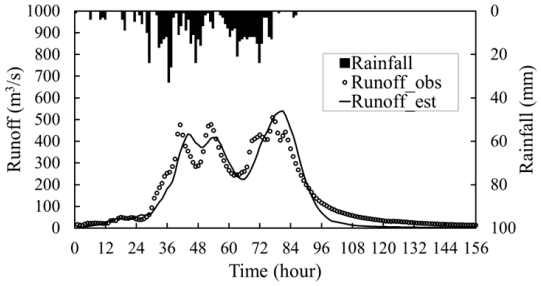
Figure 4. Locations of hydrological measurement sites and topographical features in the study area, the Keelung River.

3.2. Study Data

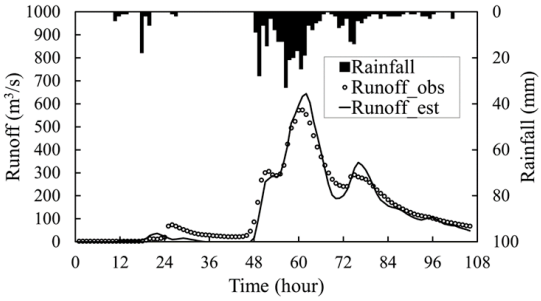
3.2.1. Rainfall-Related Factors

While configuring the proposed RA_WLTE_River model, a significant number of rainstorms should be generated by the SM_GSTR model with the statistical properties of rainfall characteristics. In the study area (the Keelung River watershed), the sub-basin rainfall characteristics are extracted from the areal-average rainfall series of 10 historical

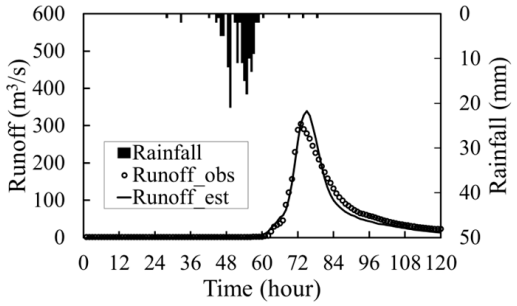
typhoon events recorded at water-level gauges that had recently caused severe floods in the study area. For example, at the WLG5 gauge (see Figure 5), the maximum rainfall intensity, on average, ranges from 40 mm/hr to 90 mm/h over durations of 60 to 120 h. Hence, the spatial and temporal uncertainties in the rainstorms should be considered when estimating the river-based water-level threshold.



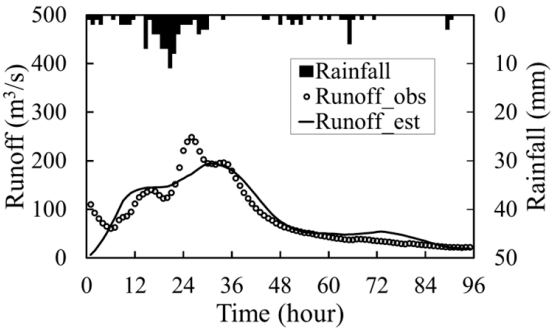
(**a**) EV1(Typhoon Sinlaku): 2008/9/12 00:00~2008/9/18 20:00



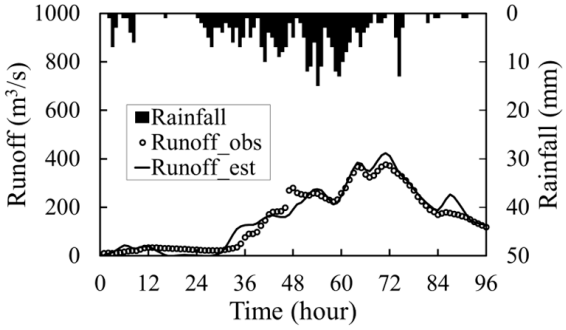
(**b**) EV2 (Typhoon Jangmi): 2008/9/26 09:00~2008/9/30 18:00



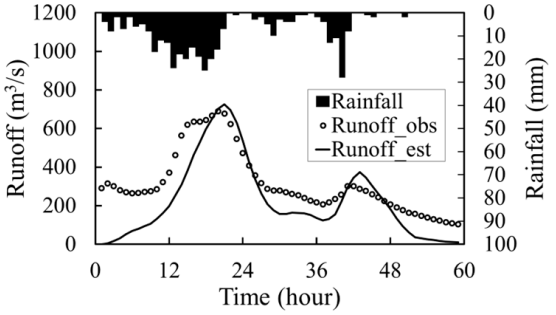
(**c**) EV3 (Typhoon Fung-wong): 2014/9/19 08:00~2014/9/22 18:00



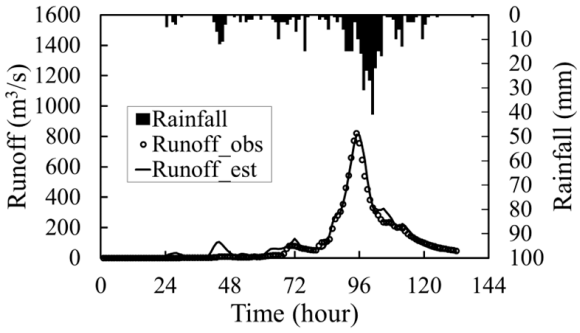
(**d**) EV4 (Typhoon Morakot): 2009/8/7 00:00~2009/8/10 22:00



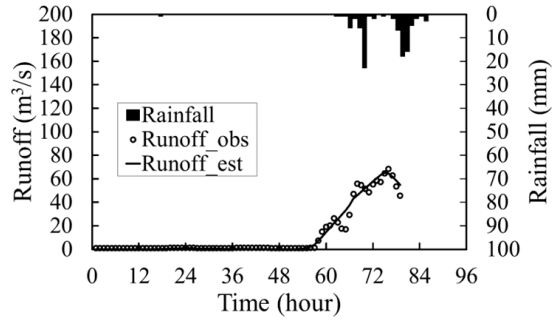
(**e**) EV5 (Typhoon Parma): 2009/10/2 00:00~2009/10/7 23:00



(**f**) EV6 (Typhoon Megi): 2010/10/21 02:00~2010/10/24 16:00

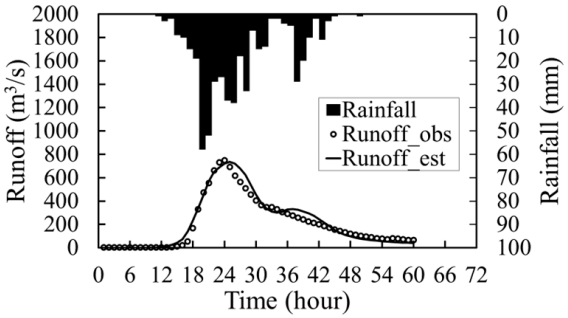


(**g**) EV7 (Typhoon Saola): 2012/7/29 09:00~2012/8/3 20:00

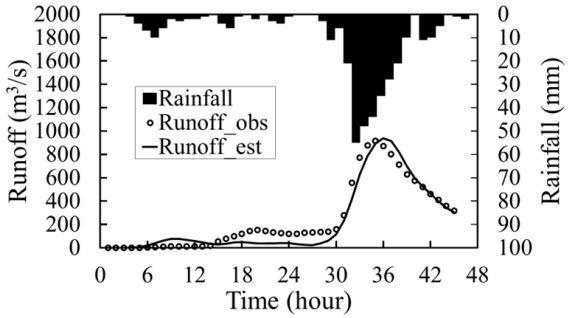


(**h**) EV8 (Typhoon Fung-wong): 2014/9/19 08:00~2014/9/22 18:00

Figure 5. *Cont.*



(**i**) EV9 (Typhoon Soudelor): 2015/8/7 12:00~2015/8/9 23:00



(**j**) EV10 (Typhoon Dujuan): 2015/9/27 12:00~2015/9/28 08:00

Figure 5. Historical hyetographs and corresponding runoffs of the ten typhoon events at the water-level gauge (WG5).

3.2.2. Runoff-Related Factors

The proposed RA_WLTE_River model includes the rainfall–runoff (SAC-SMA) model parameters, river-channel roughness coefficients, and tide depths. The data collection and analysis of the above runoff-related factors are briefly expressed in the following:

(1) SAC-SMA parameters

In the runoff estimation, the 11 parameters of the rainfall–runoff model (SAC-SMA) (see Table 1) should be calibrated to develop the proposed RA_WLTE_River model. Figure 5 illustrates that the modified GA algorithm, GA-SA, calibrated the SAC-SMA parameters using the areal-average rainfall and the corresponding runoff hydrograph recorded at the upstream water-level gauge WLG5, with high-quality observations, as listed in Table 3. Regarding Figure 4, the calibrated SAC-SMA parameters (see Table 3) accurately and reasonably capture the temporal variation in rainfall–runoff characteristics within the study area, with a high Nash–Sutcliffe coefficient (nearly 0.9) and a low ratio of difference between the estimated and the observed peak discharges (about 0.2). Moreover, the SAC-SMA parameters vary noticeably with rainstorms, with a coefficient of variation ranging from 0.23 to 1.07. This implies that the temporal uncertainties in the SAC-SMA parameters should be considered in the reliability quantification of water-level thresholds. Moreover, among the above 11 SAC-SMA parameters, UZTWM, UZK, PCTIM, ADIMP, LZTWM, DF_L, and DF_P considerably contribute to the estimation of peak discharge [46], which significantly impacts the estimated water-level threshold (see Equation (1)). Therefore, the above 7 SAC-SMA parameters are considered as runoff-related factors in the proposed RA_WLTE_River model.

(2) River-channel roughness

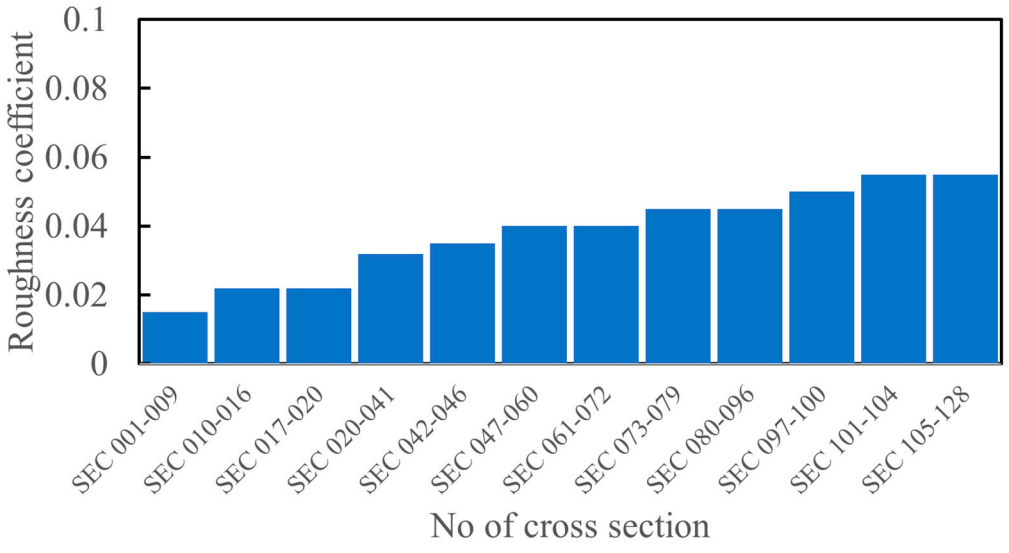
Generally, riverbed elevation and roughness play essential roles in 1D river routing, as they primarily determine the runoff that moves along a river. Figure 6a illustrates the river-channel roughness coefficients used in estimating the river stage in this study area, indicating that the roughness coefficient increases significantly with a higher distance from the estuary, from 0.01 to 0.006. Nevertheless, when separated into six elements at the 128 cross-sections, the roughness coefficients were emulated at each cross-section in the study area.

Table 3. Summary of calibrated SAC-SMA parameters for the ten typhoon events at the water-level gauge WLG5.

Event	SAC-SMA Parameters										
	UZTWM	UZFWM	UZK	PCTIM	ADIMP	ZPERC	LZTWM	LZFSM	LZSK	DF_L	DF_P
EV1	73.55	138.71	0.18	0.53	0.24	49.52	553.65	88.79	0.17	19.00	0.11
EV2	151.62	136.86	0.93	0.08	0.39	40.48	225.73	172.83	0.18	9.00	0.22
EV3	152.32	357.82	0.69	0.12	0.18	55.32	104.02	112.70	0.14	11.00	0.18
EV4	61.90	284.41	0.96	0.29	0.10	97.79	75.61	306.53	0.15	26.00	0.08
EV5	128.19	252.18	0.32	0.25	0.04	19.79	79.47	297.79	0.07	7.00	0.29
EV6	41.48	80.45	0.64	0.14	0.30	14.27	151.70	445.03	0.15	8.00	0.25
EV7	190.57	93.23	0.26	0.29	0.20	35.60	263.63	188.17	0.17	9.00	0.22
EV8	248.88	99.20	0.32	0.25	0.44	35.17	1077.26	104.38	0.18	30.00	0.07
EV9	372.60	99.11	0.20	0.31	0.11	61.92	204.29	55.07	0.20	13.00	0.15
EV10	263.15	226.99	0.93	0.26	0.13	33.03	154.76	375.92	0.16	8.00	0.25
Mean	168.43	176.90	0.54	0.25	0.21	44.29	289.01	214.72	0.16	14.00	0.18
Standard	103.41	96.56	0.32	0.12	0.13	23.86	309.79	133.64	0.04	8.21	0.08
Coefficient of variance	0.61	0.55	0.59	0.50	0.62	0.54	1.07	0.62	0.23	0.59	0.43

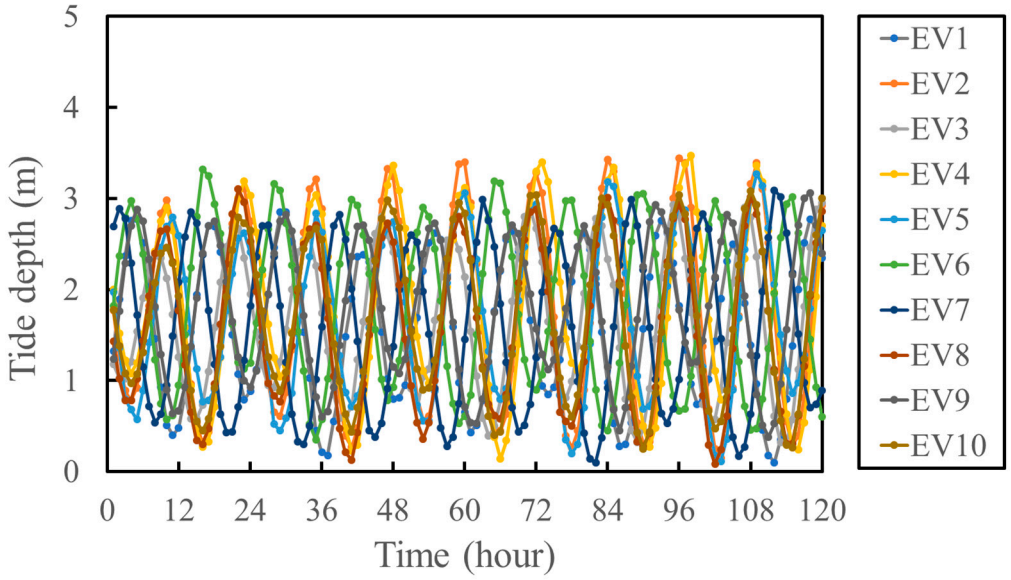
(3) Tide depth

In addition to the lateral runoffs from the sub-basins and upstream areas that are required as boundary conditions in river routing, the tide depth near the estuary is needed as the downstream boundary, which mainly contributes to the estimated river runoff and stage. Figure 6b shows the tide-depth hydrographs of 10 typhoons for 120 h, indicating that the tide depths commonly range from −1.5 m to 2.0 m, with a considerable variation in time. Therefore, to effectively respond to the impact of tide depth uncertainty on the water-level threshold, the uncertainty in tide depth is quantified using historical typhoon events and used to develop the proposed RA_WLTE_River model.



(**a**) Roughness coefficients at various cross-sections

Figure 6. *Cont.*



(**b**) Historical tide-depth hydrographs during ten typhoon events

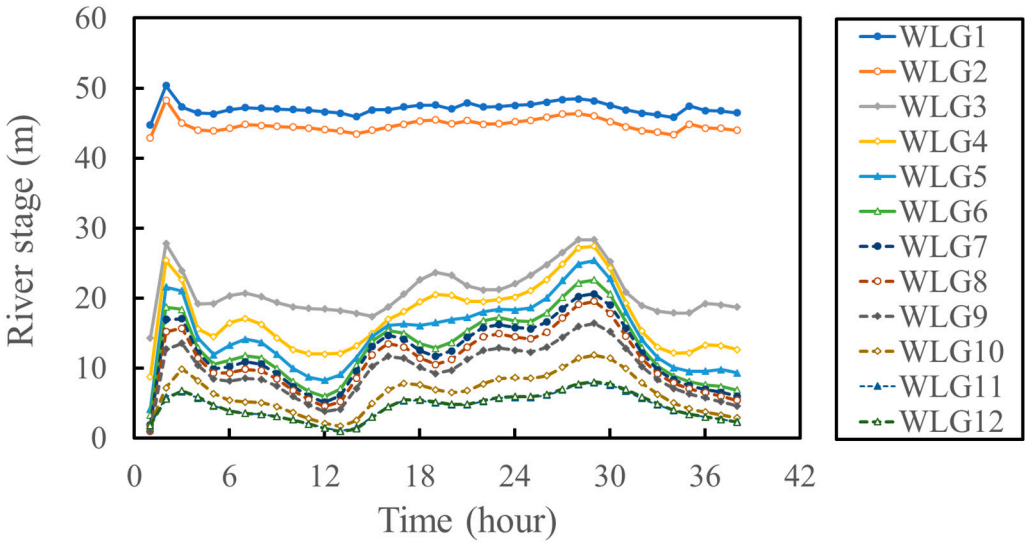
Figure 6. Historical data of riverbed roughness and tide depths in the study area.

4. Results and Discussion

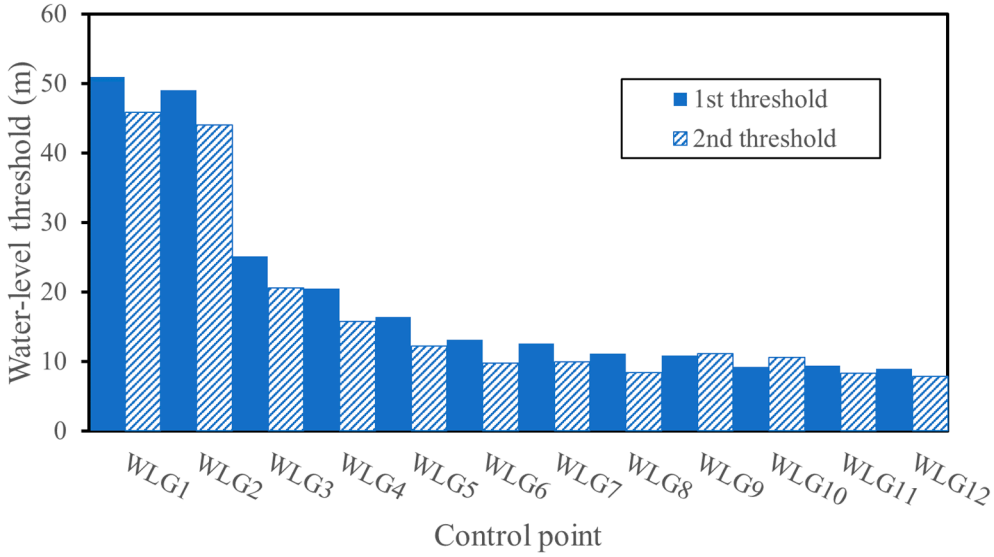
4.1. Simulation and Evaluation of the First and Second Water-Level Thresholds

Before proceeding with the simulation of river stages at various cross-sections using the SOBEK model, 1000 simulations of rainfall- and runoff-related factors should be reproduced to assess the effect of their uncertainties on the estimated water-level thresholds. In Taiwan, the warning times for river-based water-level thresholds are commonly 2 h and 5 h [36]; thus, in this study, these were defined as the first and second water-level thresholds, respectively, which can be then estimated through Equation (1) subject to the levee heights at the 12 water-level gauges (i.e., control points) (see Figure 5a) treated as the typical one (H_T). In addition, when calculating the rising rate $\left(\frac{\Delta H}{\Delta t}\right)_T$ for the first and second water-level thresholds, the differences in time (Δt) are equal to (t_P-2) and (t_P-5), respectively. Figure 7a,b illustrate ten resulting river-stage hydrographs of the first simulated event at the 12 water-level gauges (i.e., control points) and the corresponding first and second water-level thresholds, respectively.

Additionally, concerning the water-level thresholds, the first and second water-level thresholds at the 12 control points significantly increase from the downstream to the upstream under a simulated event, in which the first water-level thresholds markedly exceed the second thresholds. For example, also under the first simulated event, the first water-level thresholds markedly drop from 50.6 m (WLG1) to 8.9 m (WLG12), with the same varying trend for the second water-level thresholds, ranging from 45 m to 8 m. To quantify the variation in the first and second estimated water-level thresholds due to the uncertainties in the rainfall- and runoff-related factors, the statistical properties (i.e., mean, standard deviation, and 95% confidence interval) are calculated, as shown in Figure 8, indicating that the average first and second water-level thresholds gradually decrease from 53 m to 8 m, with standard deviations of 0.7 m and 1.5 m. This implies that the first and second water-level thresholds are affected by the above uncertainty factors, with a considerable dispersion of nearly 1 m. Notably, these factors contribute more variation to the second water-level thresholds than to the first. Therefore, the reliability of the first and second water-level thresholds must be quantified, considering uncertainties in rainfall- and runoff-related factors.



(**a**) River-stage hydrograph at 12 control points



(**b**) Water-level thresholds

Figure 7. Generated river-stage hydrograph and corresponding first and second water-level thresholds for the first simulated case.

4.2. Derivation of the Proposed RA_WLTE_River Model

4.2.1. Establishment of the Water-Level Threshold Relationship with Uncertainty Factors

It is well known that the nonlinear equation is comprehensively adopted to describe the model outputs and inputs regarding hydrological and water resources analysis [34,43]. By doing so, Equation (8) should be rewritten as

$$ln\left(H_W^{t_W}\right) = \alpha + \sum_{i=1}^{N_{UF}} \beta_i ln(\theta_i) \quad (9)$$

where $H_W^{t_W}$ and N_{UF} serve as the estimated water-level thresholds of the warning time (t_W) and the number of sensitive uncertainty factors, respectively; θ_i accounts for the uncertainty factors concerned; and α and β_i are the associated regression coefficients. As for the proposed RA_WLTE_River model, 14 rainfall- and runoff-related factors are considered, which may lead to inconsistent estimates of water-level thresholds.

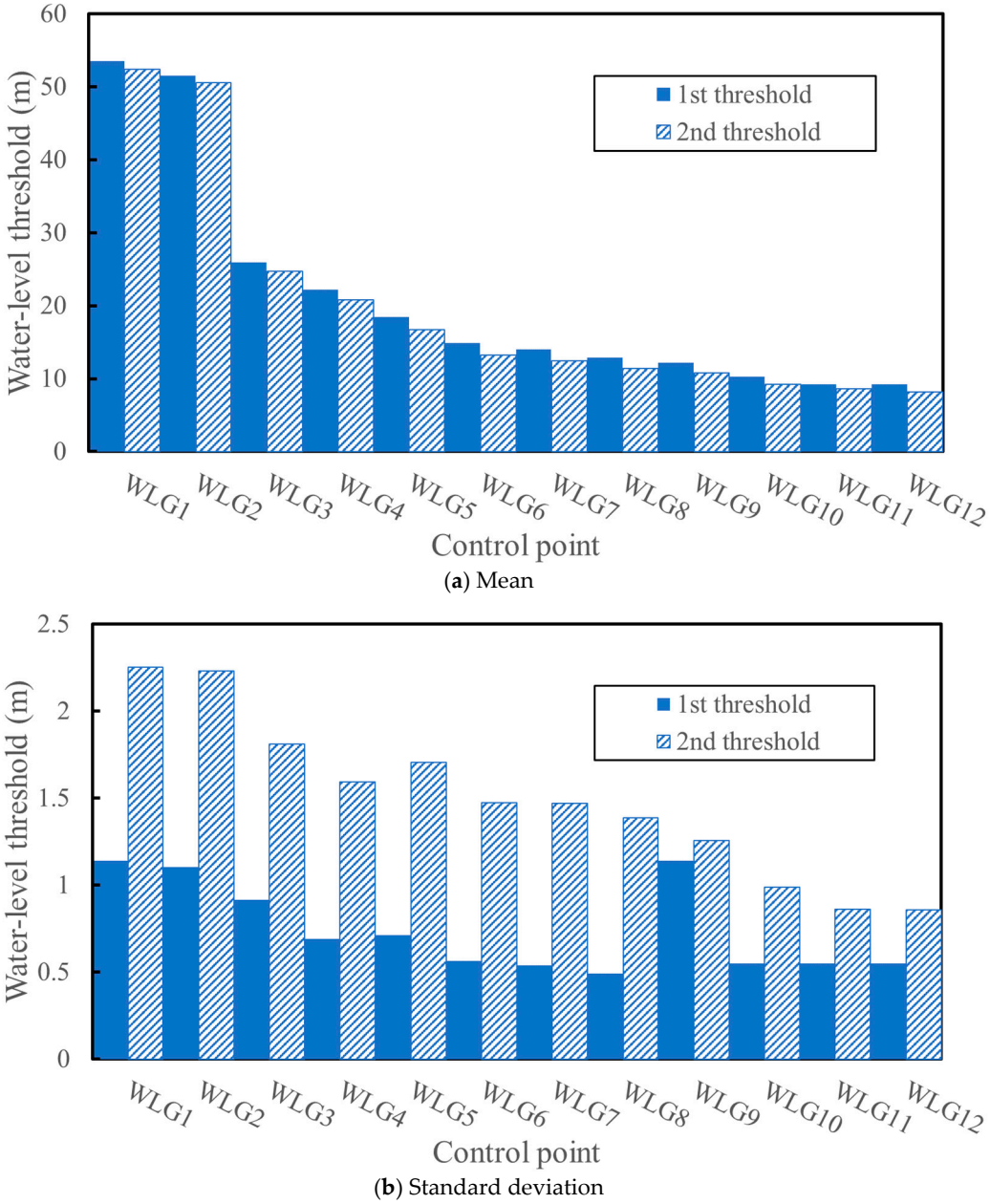


Figure 8. Statistical properties of the first and second water-level thresholds.

Regarding rainfall-related factors, the maximum river stage and its rising ratio with respect to warning time play an important role in estimating water-level thresholds using Equation (1); also, the maximum water level is mainly determined by the average rainfall and the maximum rainfall intensity [4]. Thereby, the average and maximum rainfall intensities are treated as the rainfall-related factors used in Equation (9). Additionally, the varying trend of the rainfall is probably in response to the temporal change in the river stage and runoff to the peak [46]; hence, the relative ratio of the rainfall intensity at the time step $t_p - t_w$ to the maximum intensity R_{t_p} at the time step t_p, $(\frac{R_{t_p - t_w}}{R_{t_p}})$, is defined as the rainfall-related factor in this study. In addition to rainfall-related factors, runoff-related factors are the primary contributors to river stage estimations. Indeed, the river-channel roughness coefficient and SAC-SMA parameters are required in the 1D river routing configured in the SOBEK model, indicating that these roughness coefficients and SAC-SMA should be treated as runoff-related factors. Alternatively, the maximum tide depth and the relative ratio of tide depth at the time step $\frac{TD_{t_p - t_W}}{TD_{t_p}}$, in which TD_{t_p} accounts for the maximum tide

depth at the time step t_P, are comparable to the rainfall; the relative tide depth ratio $\frac{TD_{t_P-t_W}}{TD_{t_P}}$ should be treated as a runoff-related factor.

Overall, by improving Equation (9) with the above-identified uncertainty factor, the resulting nonlinear relationship of the estimated water-level threshold can be derived via the multivariate regression analysis as

$$ln\left(H_W^{t_W}\right) = \beta_0 + \beta_1 ln(\theta_1) + \beta_2 ln(\theta_2) + \beta_3 ln(\theta_3) + \beta_4 ln(\theta_4) + \beta_5 ln(\theta_5) + \beta_6 ln(\theta_6) + \beta_7 ln(\theta_7) + \sum_{i=8}^{14} \beta_i ln(\theta_i) \quad (10)$$

where θ_1, θ_2, and θ_3 denote the average rainfall intensity, maximum rainfall intensity, and relevant ratio of rainfall intensity $\frac{R_{t_P-t_W}}{R_{t_P}}$, respectively; θ_4 denotes the river-channel roughness coefficient; θ_5, θ_6, and θ_7 denote the maximum tide depth and relative ratio of tide depth $\frac{TD_{t_P-t_W}}{TD_{t_P}}$, respectively; and $\theta_8 - \theta_{14}$ serve as the parameters of the SAC-SMA model. Table 3 shows the regression coefficients of the selected uncertainty factors, which estimate the first and second water-level thresholds at the 12 cross-sections (i.e., control points) and corresponding statistical properties (mean and standard deviation).

As shown in Table 4, among the uncertainty factors relying on rainfall-related factors (β_1–β_3), the average and maximum rainfall intensities exhibit a more pronounced contribution to the estimated water-level thresholds, with regression coefficients (0.02 and −0.059) that are, on average, more significant than the rising ratio (0.01). This implies that the heavier absolute values of the average and maximum rainfall intensities possibly result in the larger maximum river stage and the associated rising ratio, which induce a lower water-level threshold via Equation (1). As a result, the average and maximum rainfall intensities are positively and negatively related to the estimated water-level threshold.

Table 4. Regression coefficients of uncertainty factors used to estimate the water-level thresholds.

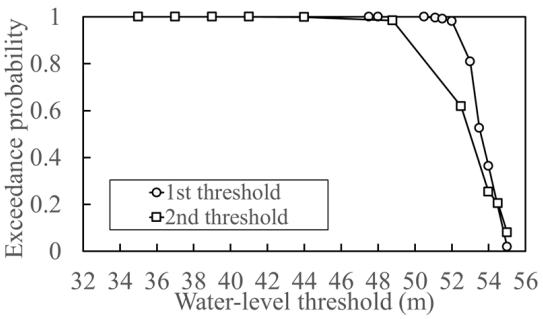
Control Point	Threshold Number	β_0	β_1	β_2	β_3	β_4	β_5	β_6	β_7	β_8	β_9	β_{10}	β_{11}	β_{12}	β_{13}	β_{14}
WLG1	First	45.912	−0.002	−0.006	0	−0.013	0.002	0.005	0.003	−0.015	−0.012	0.007	0.016	0.006	−0.005	−0.001
	Second	35.731	0.005	−0.012	0.001	−0.018	0.011	0	0.01	−0.028	−0.029	0.011	0.038	0.019	−0.005	−0.006
WLG2	First	43.943	−0.003	−0.005	0	−0.012	0.003	0.003	0.003	−0.015	−0.012	0.006	0.017	0.005	−0.004	0.001
	Second	33.326	0.002	−0.011	0.001	−0.019	0.013	0.001	0.01	−0.031	−0.03	0.011	0.041	0.018	−0.005	−0.002
WLG3	First	21.159	−0.012	−0.005	−0.001	−0.037	−0.001	0.004	0.004	−0.023	−0.017	0.005	0.022	−0.007	−0.008	0.009
	Second	12.361	0.007	−0.042	0.001	−0.034	0.006	0.013	0.011	−0.088	−0.058	0.032	0.094	−0.035	−0.057	0.106
WLG4	First	18.65	0.001	−0.024	0.003	−0.006	0.004	−0.005	0.005	−0.022	−0.014	0	0.017	0.007	0.007	−0.004
	Second	11.204	0.053	−0.091	0	−0.09	0.013	0.002	0.023	−0.078	−0.062	0.042	0.094	−0.01	−0.053	0.048
WLG5	First	18.104	0.009	−0.03	0	0.002	0.003	−0.004	0.011	−0.003	−0.013	−0.007	0.013	0.007	0.008	−0.013
	Second	10.424	0.064	−0.118	0	−0.03	−0.01	0.01	0.023	−0.054	−0.056	−0.002	0.07	0.032	0.001	−0.012
WLG6	First	13.251	0.01	−0.043	0.004	−0.002	−0.001	0	0.008	0	−0.015	−0.012	0.006	0.01	0.023	−0.012
	Second	7.788	0.087	−0.179	−0.001	−0.084	−0.037	0.011	0.02	−0.031	−0.038	−0.032	0.046	0.059	0.047	−0.051
WLG7	First	11.715	0.014	−0.047	0.007	−0.005	−0.004	−0.001	0.006	−0.01	−0.017	−0.009	0.01	0.01	0.021	−0.005
	Second	7.518	0.112	−0.211	−0.003	−0.078	−0.028	0.017	0.025	−0.038	−0.049	−0.024	0.058	0.058	0.036	−0.044
WLG8	First	12.661	0.01	−0.046	0.004	0.008	−0.004	0.004	0.007	−0.007	−0.016	−0.007	0.009	0.011	0.014	−0.014
	Second	7.61	0.106	−0.22	−0.001	−0.021	−0.038	0.017	0.022	−0.053	−0.051	−0.021	0.061	0.058	0.038	−0.038
WLG9	First	11.973	−0.005	−0.03	0.002	0.009	−0.007	−0.007	0.007	−0.01	−0.014	−0.002	0.011	0.009	0.01	−0.012
	Second	6.549	0.068	−0.139	0	−0.023	−0.026	−0.004	0.027	−0.04	−0.048	−0.025	0.055	0.064	0.049	−0.068
WLG10	First	11.588	−0.011	−0.011	0.002	0.028	−0.055	−0.003	−0.002	−0.019	−0.008	0.012	0.012	−0.009	−0.011	0.017
	Second	10.863	0.008	−0.072	0	0.031	−0.095	0.008	0.006	−0.04	−0.044	0.047	0.067	−0.023	−0.055	0.046
WLG11	First	13.189	−0.004	−0.008	0.002	0.038	−0.068	−0.028	−0.003	−0.002	0	0.006	0.003	−0.006	−0.012	0.012
	Second	19.959	0	−0.03	−0.001	0.087	−0.116	−0.01	−0.003	0.003	−0.012	0.044	0.029	−0.04	−0.062	0.037
WLG12	First	10.712	−0.014	−0.008	0.002	0.034	−0.066	−0.024	−0.004	−0.013	−0.002	0.009	0.005	−0.006	−0.005	0.02
	Second	15.108	−0.02	−0.031	0	0.076	−0.106	−0.017	−0.008	−0.018	−0.015	0.051	0.032	−0.044	−0.055	0.053
Mean	First	19.405	−0.001	−0.022	0.002	0.004	−0.016	−0.005	0.004	−0.012	−0.012	0.001	0.012	0.003	0.003	0.000
	Second	14.870	0.041	−0.096	0.000	−0.017	−0.034	0.004	0.014	−0.041	−0.041	0.011	0.057	0.013	−0.010	0.006
Stdev	First	12.370	0.009	0.017	0.002	0.022	0.029	0.011	0.005	0.008	0.006	0.008	0.006	0.008	0.012	0.012
	Second	9.925	0.046	0.076	0.001	0.057	0.047	0.011	0.011	0.025	0.016	0.032	0.022	0.042	0.045	0.052

Moreover, regarding the runoff-related factors, the related tide-depth coefficients, the maximum tide depth (β_4), and the corresponding rising ratio (β_5) are negative (on average, -0.007 and -0.025), indicating that they are inversely related to the estimated water-level thresholds; in particular, the maximum tide with higher coefficients contributes more to the estimated water-level thresholds, notably near the estuary (e.g., WGL12), where the backwater effect of tide may lead to the water level rising; therefore, lower warning water-level thresholds are needed. The remaining runoff-related factors (river-channel roughness coefficients and SAC-SMA parameters) exhibit positive changes with the estimated water-level thresholds. Thus, the estimated water-level threshold might be more significantly impacted by the channel roughness coefficients with higher regression coefficients.

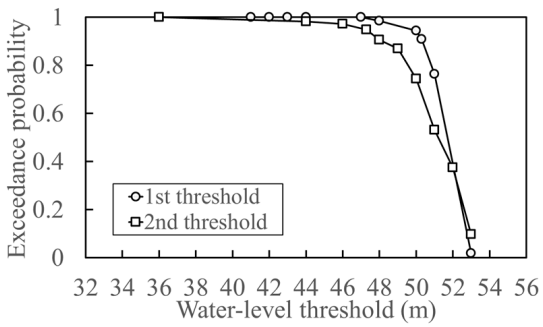
4.2.2. Reliability Quantification and Assessment of Water-Level Thresholds

Using the above nonlinear functional relationships of the 1st and 2nd water-level thresholds with the uncertainty factors (Equation (10)), the corresponding exceedance probabilities can then be computed via the AFOSM approach, with the statistical properties of the uncertainty factors (mean and variance) given in advance. Figure 9 represents the exceedance probabilities of the specific water-level thresholds, assigned based on the control elevation (see Figure 1), at the 12 water-level gauges (i.e., control points) in the study area, indicating that the exceedance probabilities significantly increase with the cross-sections located from downstream to upstream.

As shown in Figure 9, the exceedance probability of the water-level threshold shows a marked decrease with the corresponding estimates. For instance, at the control point WGL5, with the first water-level threshold rising from 8.5 m to 9.5 m, the resulting exceedance probability drops from 0.99 to 0.11; namely, the reliability significantly increases from 0.11 to 0.99. However, unlike the first water-level thresholds, the corresponding exceedance probabilities also decrease with the second water-level threshold, but with greater variation. Also, at WGL5, the water-level threshold noticeably increases from 9 m to 19 m under the exceedance probability, dropping from 0.999 to 0.003, i.e., the reliability increases from 0.0001 to 0.997. This implies that the uncertainties in the rainfall- and runoff-related factors influence the reliability of the second water-level threshold estimates in flood early warning significantly more than those of the first thresholds. Additionally, rising first and second water-level thresholds can effectively boost the corresponding reliabilities to enhance flood early warning performance.



(**a**) WGL1



(**b**) WGL2

Figure 9. *Cont.*

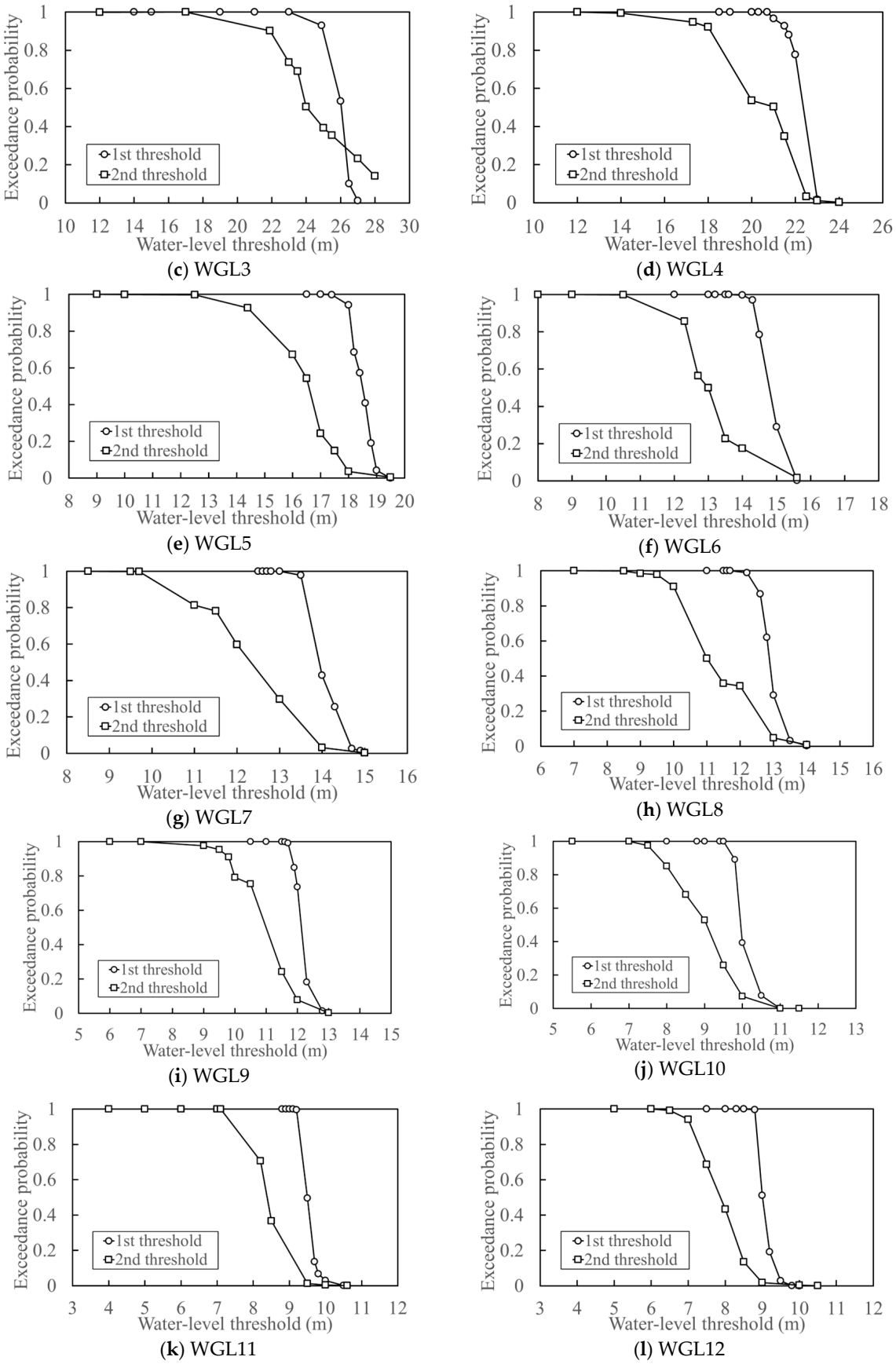


Figure 9. Exceedance probabilities of the water-level thresholds at the 12 control points via the AFOSM method in the study area.

4.2.3. Derivation of the Exceedance Probability Calculation

Within the proposed RA_WLTE_River model, to effectively proceed with quantifying the reliabilities of the water-level thresholds without carrying out the computationally expensive AFOSM method, the logistic analysis is applied to establish the exceedance-probability calculation equation (see Equation (9)). By doing so, in this study, the uncertainty factors are selected among the rainfall- and runoff-related factors with more sensitivity to the water-level threshold (see Sections 4.2.1 and 4.2.2) to create an exceedance-probability calculation equation based on the logistic regression equation (see Equation (9)) as follows:

$$ln\left[\frac{P_r\left(H_W^{t_W} > h_W^*\right)}{1 - P_r\left(H_W^{t_W} > h_W^*\right)}\right] = \alpha + \beta_1\theta_{Ravg} + \beta_2\theta_{Rmax} + \beta_3\theta_{TDmax} + \beta_4\theta_{Rough} + \beta_5\theta_{h_W^*} \quad (11)$$

where $H_W^{t_W}$ accounts for the estimated water-level threshold of the warning time t_W; θ_{Ravg} and θ_{Rmax} denote the average and maximum intensity, respectively; θ_{TDmax} and θ_{Rough} serve as the maximum tide depth and river-channel roughness coefficient, respectively; $\theta_{h_W^*}$ is the specific magnitude of the water-level threshold; and α, β_1, β_2, β_3, β_4, and β_5 are the regression coefficients as listed in Table 5. Also, the corresponding coefficient of determination (R^2) regarding Equation (11) at various control points can be seen in Figure 10, indicating that the R^2 values of the exceedance-probability calculation equations for the first and second water-level thresholds increase significantly, on average, reaching 0.83 and 0.89, respectively. It can be concluded that the derived exceedance-calculation equations are more likely to reasonably quantify the effect of the changes in the uncertainty factors on the estimated water-level thresholds.

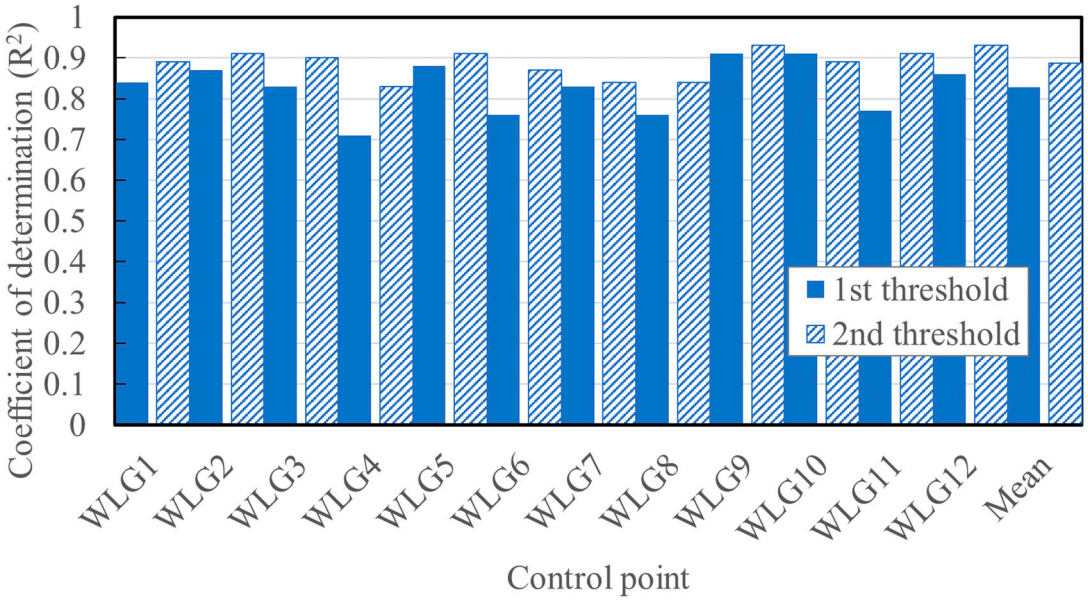


Figure 10. Coefficients of determination of exceedance-probability calculation equations at 12 control points.

In addition to the quantification of the reliabilities of the specific estimated water-level thresholds, their probabilistically based magnitudes, i.e., the estimated water-level thresholds under a desired reliability (i.e., $1 - P_r\left(H_W^{t_W} > h_W^*\right)$), can be computed by modifying Equation (11) as follows:

$$h_W^* = \frac{1}{\beta_5}\left\{\left[ln\left(\frac{P_r\left(H_W^{t_W} > h_W^*\right)}{1 - P_r\left(H_W^{t_W} > h_W^*\right)}\right)\right] - \left[\alpha + \beta_1\theta_{Ravg} + \beta_2\theta_{Rmax} + \beta_3\theta_{TDmax} + \beta_4\theta_{Rough}\right]\right\} \quad (12)$$

in which h_W^* is defined as the probabilistically based water-level thresholds. Based on the probabilistic water-level thresholds, it is expected to ensure the likelihood of achieving the goal of flood early warning at all control points.

Table 5. Regression coefficients of exceedance-probability calculation equations.

Control Point	Threshold Number	α	θ_{Ravg}	θ_{Rmax}	θ_{TDmax}	θ_{Rough}	$\theta_{h_W^*}$
WLG1	First	125.483	0.022	−0.026	−19.800	0.001	−2.313
	Second	51.523	0.065	−0.007	−10.800	−0.051	−0.968
WLG2	First	117.074	−0.074	−0.022	−17.900	0.009	−2.235
	Second	50.015	−0.040	−0.011	−31.630	0.104	−0.946
WLG3	First	50.800	−0.105	−0.014	−31.500	−0.037	−1.805
	Second	28.503	−0.028	−0.042	2.700	0.029	−1.090
WLG4	First	39.868	0.093	−0.024	5.400	0.032	−1.818
	Second	30.302	0.066	−0.058	−71.600	0.087	−1.228
WLG5	First	96.818	0.061	−0.062	6.200	0.064	−5.145
	Second	31.678	0.133	−0.069	−19.500	−0.069	−1.771
WLG6	First	40.464	0.017	−0.025	6.400	0.035	−2.579
	Second	32.813	0.251	−0.120	−35.100	−0.256	−2.212
WLG7	First	42.445	0.025	−0.040	5.500	0.098	−2.967
	Second	25.119	0.178	−0.119	−20.300	−0.131	−1.761
WLG8	First	62.669	0.011	−0.067	13.400	−0.001	−4.715
	Second	24.533	0.021	−0.115	−18.000	−0.150	−1.906
WLG9	First	82.945	−0.072	−0.081	44.600	−0.077	−6.680
	Second	33.176	0.170	−0.094	−19.800	−0.089	−2.819
WLG10	First	98.547	−0.089	−0.022	75.600	−1.058	−9.453
	Second	33.242	−0.025	−0.057	44.657	−0.511	−3.449
WLG11	First	113.398	−0.060	−0.016	119.100	−1.886	−11.414
	Second	35.613	−0.031	−0.014	90.500	−4.712	−2.794
WLG12	First	104.536	−0.208	−0.016	37.000	−1.601	−10.826
	Second	45.712	−0.059	−0.023	89.400	−0.938	−5.355

4.3. Application of the Proposed RA_WLTE_River Model on Reliability Quantification of Water-Level Thresholds

To demonstrate the applicability of the proposed RA_WLTE_River model in the reliability quantification of the first and second water-level thresholds, two application cases are given, including the historical and designed data at the upstream (WLG2), midstream (WLG5), and downstream (WLG10) control points. The detailed conditions for the two application cases above are provided in Tables 6 and 7. Also, the empirically based first and second water-level thresholds provided by the Taiwan Water Resources Agency, based on the three control elevations listed above (see Figure 4c), are adopted in the application cases.

Table 6. Conditions of rainfall- and runoff-related factors for the reliability quantification of the empirically based water-level thresholds under two historical typhoon events.

Control Point	Typhoon in 2016	Average Rainfall Intensity (mm/h)	Maximum Rainfall Intensity (mm/h)	Roughness Coefficient	Maximum Tide Depth (m)
WGL2	Megi	2	35.5	0.05	1.7
	Area	1.5	7.5	0.05	1.4
WGL5	Megi	2.7	35	0.04	1.7
	Area	1	10	0.04	1.4
WGL10	Megi	2.7	35	0.035	1.7
	Area	1	10	0.035	2.9

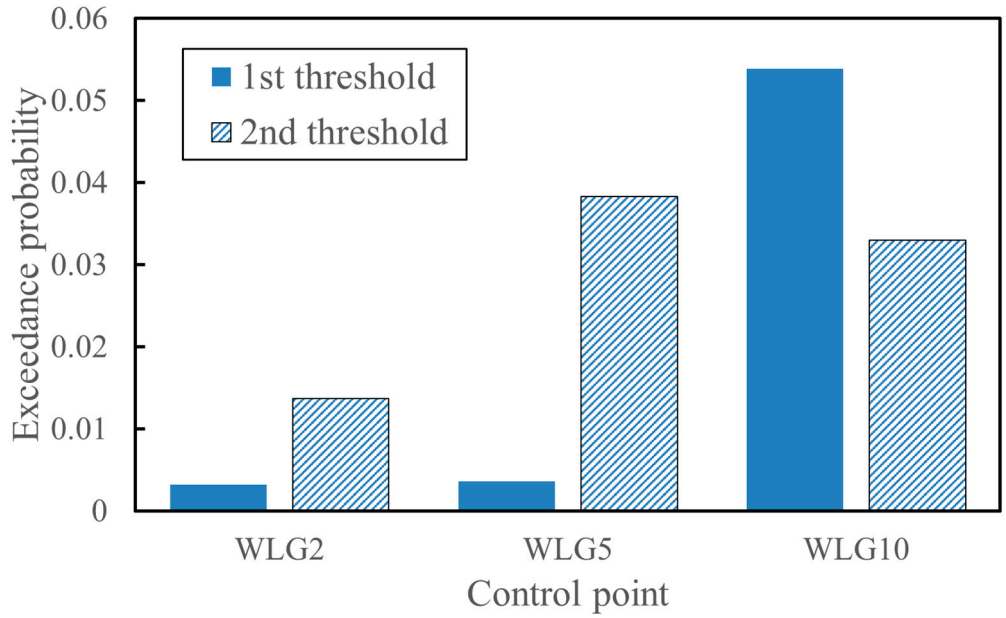
Table 7. Conditions of the uncertainty factors used in the quantification of the underestimated risk of the specific water-level thresholds under consideration of the variation in the maximum tide depth.

Control Point	Average Rainfall Intensity (mm/h)	Maximum Rainfall Intensity (mm/h)	Roughness Coefficient	Maximum Tide Depth (m)
WGL2	5	52	0.035	1
			0.035	2
			0.035	3
WGL5	5	52	0.04	1
			0.04	2
			0.04	3
WGL10	5	62	0.035	1
			0.035	2
			0.035	3

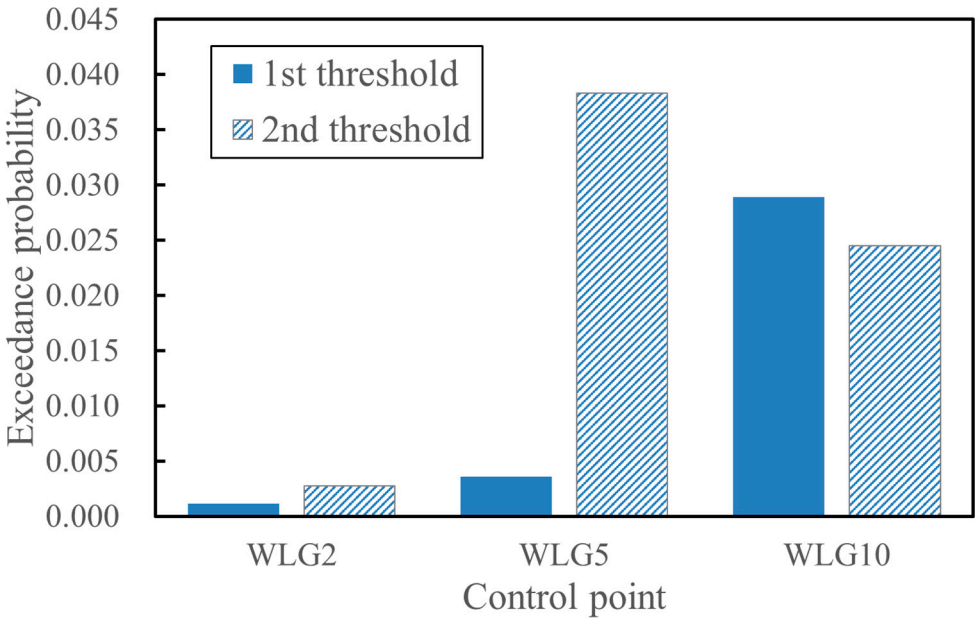
4.3.1. Historical Data

The historical data, as shown in Table 6, including the rainfall- (average and maximum rainfall intensities) and runoff-related factors (maximum tide depth and roughness coefficient), are mainly extracted from two rainstorm events in 2016, Typhoons Megi and Area. Then, via the proposed RA_WLTE_River model with the introduced estimated first and second water-level thresholds at the three control points, the corresponding exceedance probabilities can be calculated via Equation (11) (see Figure 11).

Regarding Figure 11, at the midstream and downstream control points (WGL5 and WGL10), the exceedance probabilities of the introduced first and second water-level thresholds are significantly less than 0.01, except for the second threshold at WGL5 for Typhoon Megi; namely, their reliabilities exceed 0.99. Furthermore, at the upstream control point WGL2, the exceedance probabilities of the first and second issued water-level thresholds are, on average, 0.05, with corresponding reliabilities nearly exceeding 0.95. In conclusion, the proposed RA_WLTE_River model introduces first and second water-level thresholds at control points (i.e., water-level gauges) in the study area, providing practical information for flood early warning, with a reliability exceeding 0.9.



(**a**) Typhoon Megi



(**b**) Typhoon Aere

Figure 11. Exceedance probabilities of the first and second water-level thresholds for two historical typhoon events.

4.3.2. Design Data

As well as quantifying the reliability of the officially introduced water-level thresholds, the proposed RA_WLTE_River model can also be employed to evaluate the effect of the variations in the uncertainty factors on the reliability of the estimated first and second water-level thresholds. Therefore, an application case can proceed with the proposed RA_WLTE_River model to assess the reliability of the specific water-level thresholds by varying the maximum tide depths under the remaining uncertainty factors listed in Table 6.

Figure 12 represents the exceedance probabilities of the specific first and second water-level thresholds at the downstream, midstream, and upstream control points for various

maximum depths. Specifically, at the upstream and midstream control points (WLG2 and WLG5), the corresponding exceedance probabilities to the specific first and second water-level thresholds nearly remain constant at 0.35–0.56 (i.e., reliability from 0.44 to 0.65) (WLG2) and 0.47–0.49 (i.e., reliability from 0.51 to 0.53) (WLG5). This implies that the variation in the maximum tide depth merely impacts the reliability of the water-level thresholds at the upstream and midstream control points. In contrast, the exceedance probabilities of the water-level thresholds increase significantly with tide depth, from 0.2 to 0.7 (first threshold) and from 0.46 to 0.71 (second threshold) at the downstream control point (WG10). This indicates that the tide depth likely increases the reliability of the estimated water-level thresholds (from 0.8 to 0.3 on average). Thereby, variations in tide depths might reduce the reliability of early flood alerting by 25%. By doing so, introducing the gauged first and second water-level thresholds should consider the uncertainty of the tide depth, especially at the control point near the estuary.

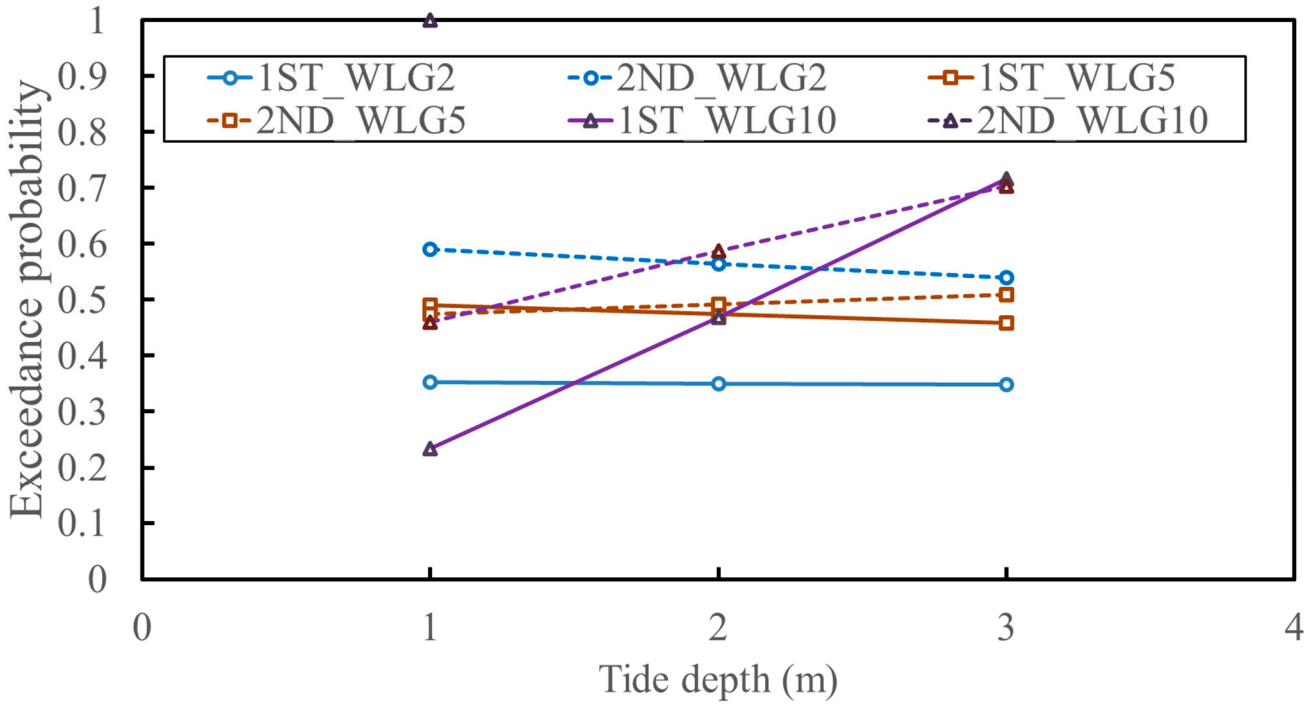


Figure 12. Exceedance probabilities of the specific water-level thresholds at 12 control points under different maximum tide depths.

4.4. Estimation of the Probabilistically Based Water-Level Thresholds

According to the above application results, the officially introduced water-level thresholds can, on average, efficiently alter rainfall-induced floods, with a high reliability of nearly 0.9. However, the reliability of the water-level thresholds varies significantly across control points, resulting in inconsistent early warning efficiency under conservative thresholds. To determine the first and second water-level thresholds for a specified reliability level, probabilistically based water-level thresholds can be estimated using Equation (12), given the rainfall- and runoff-related factors of interest.

Figure 13 exhibits the estimated first and second water-level thresholds with a reliability of 0.8 under a given average and maximum rainfall intensities (20 mm/h and 50 mm/h), roughness coefficients, and maximum tide depth (1 m); note that the roughness coefficients at the 12 control points are assigned based on the measurements (see Figure 6a), including 0.005 (WGL1-WGL3), 0.04 (WGL4-WGL5), 0.032 (WGL6-WGL9), and 0.015 (WGL10-WGL12). In Figure 12, the probabilistically based first and second

water-level thresholds at the 12 control points are clearly lower than the corresponding control elevations.

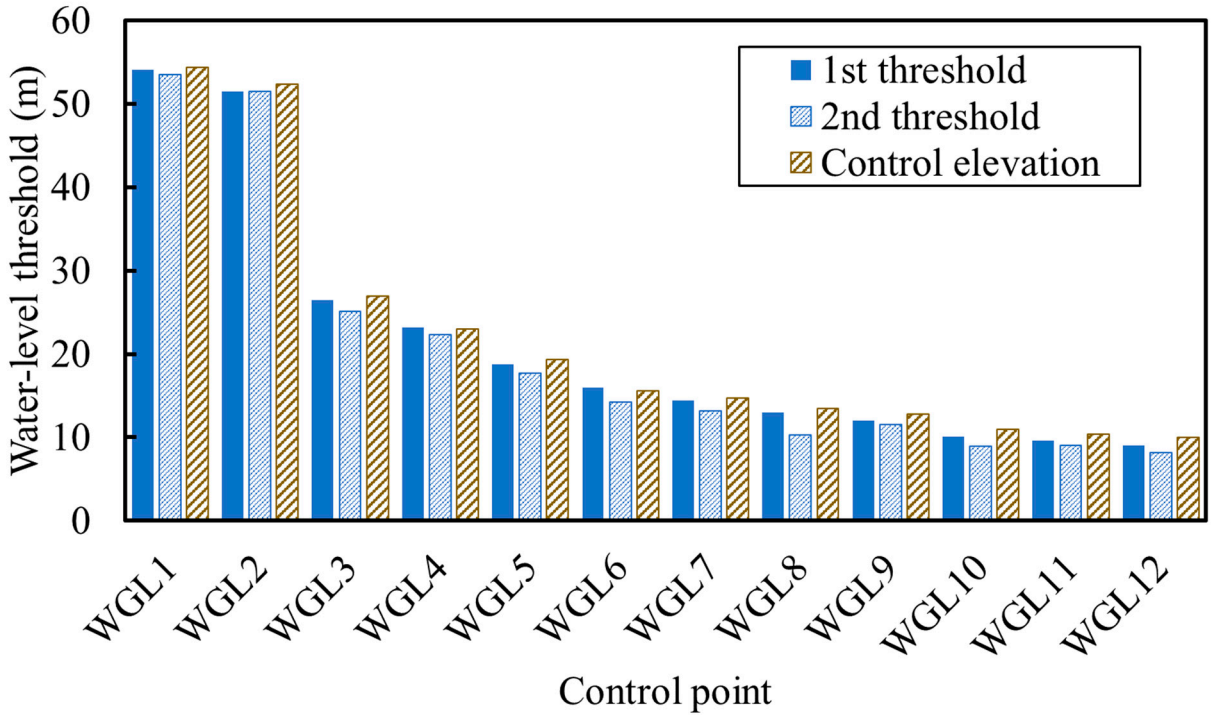


Figure 13. Illustration of the probabilistically based first and second water-level thresholds at various control points via the proposed RA_WLTE_River model with a desired reliability of 0.8.

The proposed RA_WLTE_River model can estimate more realistic water-level thresholds using the derived exceedance-probability calculation equations under a desired reliability for the rainfall- and runoff-related factors considered. Thus, rainfall-induced floods are more likely to be reliably and efficiently alerted, using probabilistically based water-level thresholds; thus, the model is advantageous for flood-control hydraulic structures, especially for levee-created systems.

5. Conclusions

This study aims to develop a risk analysis for river-based water-level thresholds, accounting for uncertainties in 14 rainfall- and runoff-related factors, referred to as the RA_WLTE_River model. The model development and demonstration results indicate that the early alert-based reliability of the introduced water-level thresholds can be reasonably and effectively quantified and analyzed using the proposed RA_WLTE_River model in response to variations in uncertainty factors across various control points. In short, the channel-based roughness coefficient contributes more significantly to the water-level estimation than the other uncertainty factors of interest. Also, at downstream control points, variations in tide depth significantly reduce early alerting efficiency and reliability by 15%. Nevertheless, the reliabilities in altering the early rainfall-induced flood based on the officially introduced water-level thresholds in the study area noticeably exceed 0.9, but with a significant spatial change; therefore, to improve the abovementioned inconsistent flood warning performance due to the conservative water-level thresholds, probabilistic-based thresholds should be provided via the proposed RA_WLTE_River model under a desired reliability for all control points along the river. As a result, the proposed RA_WLTE_River model can efficiently assess the reliability of the introduced

water-level thresholds and issue water-level thresholds with an acceptable likelihood at the locations along the river concerned.

Nonetheless, the proposed RA_WLTE_River model can provide probabilistic-based water-level thresholds to achieve a desired reliability; however, its early warning performance should be evaluated by comparing the observed river stages with the estimated probabilistic-based water-level thresholds during real rainfall-induced floods. In addition, a group of uncertainty factors is considered in the proposed RA_WLTE_River model. However, the model development might still need to consider other hydrological and hydraulic variables related to water-level estimation (e.g., riverbed stability, land use, and the lag effect of river runoff) [47–49]; it would be helpful to evaluate the impact of long-term varying trends of the hydrological variables (e.g., precipitation and runoff) [50]. Accordingly, the proposed RA_WLTE_River model may be limited by the absence of the aforementioned uncertainty factors, which likely affect the reliability of the water-level threshold. Hence, considering additional uncertainty factors would help improve the reliability quantification performance of the proposed RA_WLTE_River model. In addition, within the proposed RA_WLTE_River model, the relationship between the water-level thresholds and uncertainty factors should be known in advance, which might utilize inappropriate functional forms. However, artificial intelligence (AI) techniques are widely used to model nonlinear relationships in hydrological and hydraulic processes [51,52]. Therefore, the proposed RA_WLTE_River model would be improved by adopting an AI-derived water-level threshold estimation equation to provide more realistic thresholds than the nonlinear regression equation.

Author Contributions: S.-J.W.: conceptualization, methodology, experimental investigation, data analysis, writing, review, and editing. H.-W.Y. and S.-H.Y.: experimental work and data analyses. K.-C.Y.: data curation and experimental work. All authors have read and agreed to the published version of the manuscript.

Funding: This published paper was funded by the National United University Project (grant 114-NUUPRJ-01).

Data Availability Statement: Data cannot be shared openly but is available on request from the corresponding author (Shiang-Jen Wu).

Conflicts of Interest: The authors declare no conflicts of interest.

References

1. Zang, Y.; Meng, Y.; Guan, X.; Lv, H.; Yan, D. Study on urban flood early warning system considering flood loss. *Int. J. Disaster Risk Reduct.* **2022**, *77*, 103042. [CrossRef]
2. Marin-Perez, R.; García-Pintado, J.; Gómez, A.S. A real-time measurement system for long-life flood monitoring and warning applications. *Sensors* **2012**, *12*, 4213–4236. [CrossRef]
3. Jang, J.H. An advanced method to apply multiple rainfall thresholds for urban flood warnings. *Water* **2015**, *7*, 6056–6078. [CrossRef]
4. Wu, S.J.; Hsu, C.T.; Lien, H.C.; Chang, C.H. Modeling the effect of uncertainties in rainfall characteristics on flash flood warning based on rainfall thresholds. *Nat. Hazards* **2015**, *75*, 1677–1771. [CrossRef]
5. Hassan, W.H.W.; Jidin, A.Z.; Aziz, S.A.C.; Rahim, N. Flood disaster indicator of water level monitoring system. *Int. J. Comput. Eng.* **2019**, *19*, 1694–1699. [CrossRef]
6. Hu, Y.; Wang, Z.; Zhou, B.; Jiang, S. Analysis of the specific water level of flood control and the threshold value of rainfall warning for small and medium rivers. *Proc. Int. Assoc. Hydrol. Sci.* **2020**, *383*, 201–211. [CrossRef]
7. Ufuoma, G.; Sasanya, B.F.; Abaje, P.; Awodutire, P. Efficiency of camera sensors for flood monitoring and warnings. *Sci. Afr.* **2021**, *13*, e00887. [CrossRef]
8. Reis GdCd Pereira, T.S.R.; Faria, G.S.; Formiga, K.T.M. Analysis of the Uncertainty in Estimates of Manning's Roughness Coefficient and Bed Slope Using GLUE and DREAM. *Water* **2020**, *12*, 3270. [CrossRef]

9. Levin, S.; Briggs, M.A.; Foks, S.S.; Goodling, P.J.; Raffensperger, J.P.; Rosenberry, D.O.; Scholl, M.A.; Tiedeman, C.R.; Webb, R.M. Uncertainties in measuring and estimating water-budget components: Current state of the science. *Wiley Interdiscip. Rev. Water* **2023**, *10*, e1646. [CrossRef]
10. Wang, W.C.; Zhao, Y.W.; Chau, K.W.; Xu, D.M.; Liu, C.J. Improving flood forecasting using geomorphic unit hydrograph based on spatially distributed velocity field. *J. Hydroinform.* **2021**, *123*, 724–739. [CrossRef]
11. Wu, S.J.; Hsu, C.T.; Shen, J.C.; Chang, C.H. Modeling the 2D Inundation Simulation Based on the ANN-Derived Model with Real-Time Measurements at Roadside IoT Sensors. *Water* **2022**, *14*, 2189. [CrossRef]
12. Tu, Y.; Zhao, Y.; Meng, L.; Tang, W.; Xu, W.; Tian, J.; Lyu, G. Study on Dynamic Early Warning of Flash Floods in Hubei Province. *Water* **2023**, *15*, 3153. [CrossRef]
13. Liu, S.; Shi, X.; Liu, Q.; Tan, J.; Sun, Y.; Liu, Q.; Guo, H. Warning water level determination and its spatial distribution in coastal areas of China. *Nat. Hazards Earth Syst. Sci.* **2023**, *23*, 127–138. [CrossRef]
14. Wang, W.C.; Zhao, Y.W.; Xu, D.M.; Hong, Y.G. Error correction method based on deep learning for imporving the accuracy of conceptual rainfall runoff model. *J. Hydrol.* **2024**, *643*, 131992.
15. Dutta, D.; Alam, J.; Umeda, K.; Hayashi, M.; Hironaka, S. A two-dimensional hydrodynamic model for flood inundation simulation: A case study in the lower Mekong river basin. *Hydrol. Process.* **2007**, *21*, 1223–1237. [CrossRef]
16. Clark, R.A.; Gourley, J.J.; Flamig, Z.L.; Hong, Y.; Clark, E. CONUS-wide evaluation of national weather service flash flood guidance products. *Weather. Forecast.* **2014**, *29*, 377–392. [CrossRef]
17. Ming, X.; Liang, Q.; Xia, X.; Li, D.; Fowler, H.J. Real-time flood forecasting based on a high-performance 2-D hydrodynamic model and numerical weather predictions. *Water Resour. Res.* **2020**, *56*, e2019WR025583. [CrossRef]
18. Kalimisetty, S.; Singh, A.; Venkata, D.R.K.H. 1D and 2D model coupling approach for the development of operational spatial flood early warning system. *Geocarto Int.* **2021**, *37*, 4390–4405. [CrossRef]
19. Szeląg, B.; Suligowski, R.; Drewnowski, J.; De Paola, F.; Fernandez-Morales, F.J.M.; Bask, L. Simulation of the number of storm overflows considering changes in precipitation dynamics and the urbanization of the catchment area: A probabilistic approach. *J. Hydrol.* **2021**, *598*, 126275. [CrossRef]
20. Mitsopoulos, G.; Panagiotatou, E.; Sant, V.; Baltas, E.; Diakakis, M.; Lekkas, W.; Stamou, A. Optimizing the Performance of Coupled 1D/2D Hydrodynamic Models for Early Warning of Flash Floods. *Water* **2022**, *14*, 2356. [CrossRef]
21. Hosseiny, H. A deep learning model for predicting river flood depth and extent. *Environ. Model. Softw.* **2021**, *145*, 105186. [CrossRef]
22. Lu, W.; Xia, W.; Shoemaker, C.A. Surrogate global optimization for identifying cost-effective green infrastructure for urban flood control with a computationally expensive inundation model. *Water Resour. Res.* **2022**, *58*, e2021WR030928. [CrossRef]
23. Mehedi, M.A.A.; Smith, V.; Hosseiny, H.; Jiao, X. Unraveling the complexities of urban fuvial food hydraulics through AI. *Sci. Rep.* **2022**, *12*, 18378. [CrossRef]
24. Bout, B.V.D.; Jetten, V.G.; van Westen, C.J.; Lombardo, L. A breakthrough in fast flood simulation. *Environ. Model. Softw.* **2023**, *168*, 105787. [CrossRef]
25. Guo, W.D.; Chen, W.B.; Yeh, S.H.; Chang, C.H.; Chen, H. Prediction of River Stage Using Multistep-Ahead Machine Learning Techniques for a Tidal River of Taiwan. *Water* **2021**, *13*, 920. [CrossRef]
26. Isizoh, A.H.; Nwani, E.M.; Onyia, T.C.; Eze, C.E.; Okeke, N.P. Real-Time Flood Monitoring and Early Warning System Using Artificial Intelligence Technique. *Int. J. Adv. Eng. Manag.* **2021**, *3*, 2287–2300.
27. Munoz, P.; Orellana-Alvear, J.; Bendix, J.; Feyen, J.; Celleri, R. lood Early Warning Systems Using Machine Learning Techniques: The Case of the Tomebamba Catchment at the Southern Andes of Ecuador. *Hydrology* **2021**, *8*, 183. [CrossRef]
28. Sanders, W.; Li, D.; Li, W.; Fang, Z. Data-driven flood alert System (FAS) Using extreme gradient boosting (XGBoost) to forecast flood stages. *Water* **2022**, *14*, 747. [CrossRef]
29. Moon, H.; Yoon, S.; Moon, Y. Urban flood forecasting using a hybrid modeling approach based on a deep learning technique. *J. Hydroinform.* **2023**, *25*, 593. [CrossRef]
30. Adikari, K.E.; Shrestha, S.; Ratnayake, D.; Budhathoki, A.; Mohanasundaram, S.; Dailey, M.N.; Budhathoki, A.; Mohanasundaram, S.; Dailey, M.N. valuation of artificial intelligence models for flood and drought forecasting in arid and tropical regions. *Environ. Model. Softw.* **2021**, *144*, 105136. [CrossRef]
31. Wu, S.J.; Hsu, C.T.; Chang, C.H. Stochastic modeling of gridded short-term rainstorms. *Hydrol. Res.* **2021**, *52*, 876–904. [CrossRef]
32. Kumar, V.; Azamathulla, H.M.; Sharma, K.V.; Mehta, D.J.; Maharaj, K.T. The State of the Art in Deep Learning Applications, Challenges, and Future Prospects: A Comprehensive Review of Flood Forecasting and Management. *Sustainability* **2023**, *15*, 10543. [CrossRef]
33. Hauswirth, S.M.; van der Wiel, K.; Bierkens, M.F.P.; Beijk, V.; Wanders, N. Simulating hydrological extremes for different warming levels–combining large scale climate ensembles with local observation based machine learning models. *Front. Water* **2023**, *5*, 1108108. [CrossRef]

34. Wu, S.J.; Yang, J.C.; Tung, Y.K. Risk analysis for flood-control structure under consideration of uncertainties in design flood. *Nat. Hazards* **2011**, *58*, 117–140. [CrossRef]
35. Chang, C.H.; Yang, J.C.; Tung, Y.K. Incorporate marginal distributions in point estimate methods for uncertainty analysis. *J. Hydraul. Eng.* **1997**, *123*, 244–251. [CrossRef]
36. Yang, S.H.; Yeh, K.C. Establishment and Practical Application of Flood Warning Stage in Taiwan's River. *Geophys. Res. Abstr.* **2017**, *19*, EGU2017-8219.
37. Deltares systems. *SOBEK 1D/2D modelling suite for integral water solutions User Manual*; Delftares: Delft, The Netherlands, 2023; Available online: https://content.oss.deltares.nl/sobek2/SOBEK_User_Manual.pdf (accessed on 24 October 2025).
38. Wu, S.J.; Lien, H.C.; Chang, C.H. Calibration of Conceptual Rainfall-Runoff Model using Genetic Algorithm Integrated with Runoff Estimation sensitivity to parameters. *J. Hydroinform.* **2012**, *14*, 497–511. [CrossRef]
39. Tung, Y.K.; Yeh, K.C. Evaluation of safety of hydraulic structures affected by migrating pits. *Stoch. Hydrol. Hydraulic.* **1993**, *7*, 131–145. [CrossRef]
40. Tung, Y.K.; Yen, B.C. *Hydrosystems Engineering Uncertainty Analysis*; McGrqw-Hill Company: New York, NY, USA, 2005.
41. Ganji, A.; Jowkarshorijeh, L. Advance first order second moment (AFOSM) method for single reservoir operation reliability analysis: A case study. *Stoch. Environ. Risk Assess.* **2012**, *26*, 33–42. [CrossRef]
42. Gabriel-Martin, I.; Sordo-Ward, A.; Garrote, L.; Castillo, L.G. Influence of initial reservoir level and gate failure in dam safety analysis. Stochastic approach. *J. Hydrol.* **2017**, *550*, 669–684. [CrossRef]
43. Tung, Y.K. Uncertainty and reliability analysis in water resources engineering. *J. Contemp. Water Res. Educ.* **2011**, *103*, 13–21.
44. Lee, J.; Kim, B. Scenario-based real-time flood prediction with logistic regression. *Water* **2021**, *13*, 1191. [CrossRef]
45. Li, Y.; Ding, C.; Yu, H.; Zhou, W.H.; Peng, S. Quantitative evaluation of life loss induced by embankment failure with the impact of riverbed deformation. *Int. J. Disaster Risk Reduct.* **2025**, *120*, 105390. [CrossRef]
46. Wu, S.J.; Lien, H.O.; Chang, C.H. Modeling risk analysis for forecasting peak discharge during flooding prevention and warning operation. *Stoch. Environ. Res. Risk Assess.* **2010**, *24*, 1175–1191. [CrossRef]
47. Sivakuma, B.; Singh, V.P. Hydrologic system complexity and nonlinear dynamic concepts for a catchment classification framework. *Hydrol. Earth Syst. Sci. Discuss.* **2022**, *8*, 4427–4458.
48. Higashino, M.; Stefan, H. Variability and change of precipitation and flood discharge in a Japanese river basin. *J. Hydrol. Reg. Stud.* **2019**, *21*, 68–79. [CrossRef]
49. Ma, K.; He, D.; Liu, S.; Ji, X.; Li, Y.; Jiang, H. Novel time-lag informed deep learning framework for enhanced streamflow prediction and flood early warning in large-scale catchments. *J. Hydrol.* **2024**, *631*, 130841. [CrossRef]
50. Hooshyaripor, F.; Faraji-Ashkavar, S.; Koohyian, F.; Tang, Q.; Noori, R. Annual flood damage influenced by El Niño in the Kan River basin, Iran. *Nat. Harards Earth Syst. Sci.* **2020**, *20*, 2739–2751. [CrossRef]
51. Alasali, F.; Tawalbeh, R.T.; Ghanem, Z.; Mohammad, F.; Alghazzawi, M. A Sustainable Early Warning System Using Rolling Forecasts Based on ANN and Golden Ratio Optimization Methods to Accurately Predict Real-Time Water Levels and Flash Flood. *Sensor* **2021**, *21*, 4598. [CrossRef]
52. Sušanj Cule, I.; Ožani'c, N.; Volf, G.; Karleuša, B. Artificial Neural Network (ANN) Water-Level Prediction Model as a Tool for the Sustainable Management of the Vrana Lake (Croatia) Water Supply System. *Sustainability* **2025**, *17*, 722. [CrossRef]

Disclaimer/Publisher's Note: The statements, opinions and data contained in all publications are solely those of the individual author(s) and contributor(s) and not of MDPI and/or the editor(s). MDPI and/or the editor(s) disclaim responsibility for any injury to people or property resulting from any ideas, methods, instructions or products referred to in the content.